Article

Cell Chemical Biology

Ferroptosis inhibition by oleic acid mitigates iron-overload-induced injury

Graphical abstract

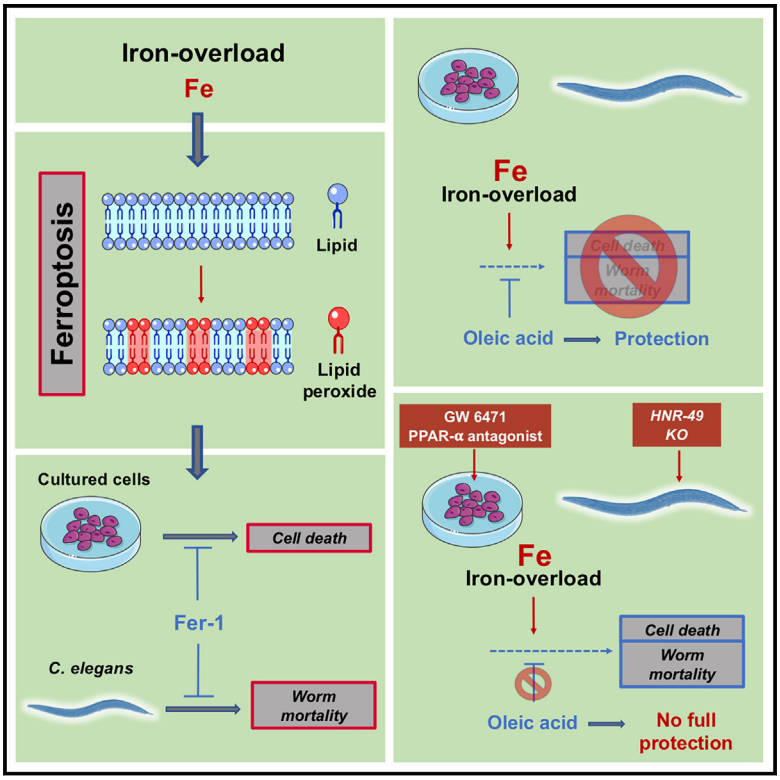

Authors

Josiane Mann, Eduard Reznik, Melania Santer, ..., Antonio Miranda-Vizuete, Marcelo Farina, Brent R. Stockwell

Correspondence

marcelo.farina@ufsc.br (M.F.), bstockwell@columbia.edu (B.R.S.)

In brief

Mann et al. identify the occurrence of ferroptosis in the context of iron overload-mediated injury in cultured human cell lines, *C. elegans* and mice. Exogenous oleic acid suppressed ferroptosis and protected against iron overload-induced injury, highlighting its potential use to mitigate organ damage observed in iron overload individuals.

Highlights

- Iron overload causes ferroptosis in kidney, hepatic, and neuronal cell lines
- Iron overload causes ferroptosis-driven damage and mortality in *C. elegans*
- Oleic acid blocks iron-overload-induced damage by inhibiting ferroptosis
- Oleic acid inhibits iron-overload-induced liver lipid peroxidation and damage in mice

Mann et al., 2024, Cell Chemical Biology *31*, 1–16
February 15, 2024
https://doi.org/10.1016/j.chembiol.2023.10.012

CellPress

Please cite this article in press as: Mann et al., Ferroptosis inhibition by oleic acid mitigates iron-overload-induced injury, Cell Chemical Biology (2023), https://doi.org/10.1016/j.chembiol.2023.10.012

Cell Chemical Biology

CellPress

Article

Ferroptosis inhibition by oleic acid mitigates iron-overload-induced injury

Josiane Mann,[1,8] Eduard Reznik,[2,8] Melania Santer,[1] Mark A. Fongheiser,[2] Nailah Smith,[2] Tal Hirschhorn,[2] Fereshteh Zandkarimi,[5] Rajesh Kumar Soni,[3] Alcir Luiz Dafré,[1] Antonio Miranda-Vizuete,[4] Marcelo Farina,[1,2,*] and Brent R. Stockwell[2,3,5,6,7,9,*]

[1]Department of Biochemistry, Federal University of Santa Catarina, Florianópolis, Santa Catarina 88040-900, Brazil
[2]Department of Biological Sciences, Columbia University, New York, NY 10027, USA
[3]Herbert Irving Comprehensive Cancer Center, Columbia University, New York, NY 10032, USA
[4]Instituto de Biomedicina de Sevilla, IBiS/Hospital Universitario Virgen del Rocío/CSIC/Universidad de Sevilla, 41013, Seville, Spain
[5]Department of Chemistry, Columbia University, New York, NY 10027, USA
[6]Irving Institute for Cancer Dynamics, Columbia University, New York, NY 10027, USA
[7]Department of Pathology and Cell Biology, Vagelos College of Physicians and Surgeons, Columbia University Irving Medical Center, New York. NY 10032, USA
[8]These authors contributed equally
[9]Lead contact
*Correspondence: marcelo.farina@ufsc.br (M.F.), bstockwell@columbia.edu (B.R.S.)
https://doi.org/10.1016/j.chembiol.2023.10.012

SUMMARY

Iron overload, characterized by accumulation of iron in tissues, induces a multiorgan toxicity whose mechanisms are not fully understood. Using cultured cell lines, *Caenorhabditis elegans,* and mice, we found that ferroptosis occurs in the context of iron-overload-mediated damage. Exogenous oleic acid protected against iron-overload-toxicity in cell culture and *Caenorhabditis elegans* by suppressing ferroptosis. In mice, oleic acid protected against FAC-induced liver lipid peroxidation and damage. Oleic acid changed the cellular lipid composition, characterized by decreased levels of polyunsaturated fatty acyl phospholipids and decreased levels of ether-linked phospholipids. The protective effect of oleic acid in cells was attenuated by GW6471 (PPAR-α antagonist), as well as in *Caenorhabditis elegans* lacking the nuclear hormone receptor NHR-49 (a PPAR-α functional homologue). These results highlight ferroptosis as a driver of iron-overload-mediated damage, which is inhibited by oleic acid. This monounsaturated fatty acid represents a potential therapeutic approach to mitigating organ damage in iron overload individuals.

INTRODUCTION

Iron overload disorders, which encompass primary and secondary iron overload, represent an important class of human diseases characterized by excess iron in the body.[1] Primary iron overload results from mutations in genes encoding key elements involved in iron homeostasis, such as hemochromatosis protein (HFE),[2] hemojuvelin (HJV),[3] transferrin receptor 2 (TFR2),[4] ferroportin (SLC11A3),[5] and hepcidin (HAMP).[6] Secondary iron overload results mainly from frequent blood transfusions in patients with hematological disorders.[1] In addition, there are other forms of iron overload with variable etiologies, including iron overdose (acute iron poisonings), which has been described after accidental ingestion of iron-containing syrups by children or suicidal poisoning.[7–10] Excess plasma iron has also been found to mediate multiorgan failure, a common cause of death in the ICU.[11] Although it is well known that iron overload causes substantial toxicity to diverse organs, such as liver, heart, kidney, and brain,[12–15] the molecular mechanisms mediating such toxicity are not completely understood. However, a recent study reported that the severity of multiorgan dysfunction and the probability of death is associated with both catalytic iron levels and excessive lipid peroxidation (a ferroptosis marker) in critically ill patients.[11]

Ferroptosis is an iron-driven form of regulated cell death caused by the oxidation of membrane phospholipids.[16] Within the last decade, a growing body of evidence has indicated that such a *driver* role of iron-dependent lipid peroxidation in ferroptosis is regulated by several metabolic pathways, including iron and redox homeostasis, mitochondrial activity, and metabolism of amino acids, carbohydrates, and lipids.[17] Ferroptosis has significant roles in renal,[18] hepatic,[19,20] and cerebral[21,22] pathological conditions, among others. Of note, iron-chelating agents, which have been valuable in the treatment of iron overload,[23,24] have also exhibited beneficial effects in experimental models elicited by classic ferroptosis inducers, such as erastin,[25] RSL3,[26] and glutathione depletion.[27] However, whether ferroptosis is necessary for iron-overload pathology is unclear.

Lipids, which have vital functions in the maintenance of cellular homeostasis due to their roles as major metabolic energy stores

Please cite this article in press as: Mann et al., Ferroptosis inhibition by oleic acid mitigates iron-overload-induced injury, Cell Chemical Biology (2023), https://doi.org/10.1016/j.chembiol.2023.10.012

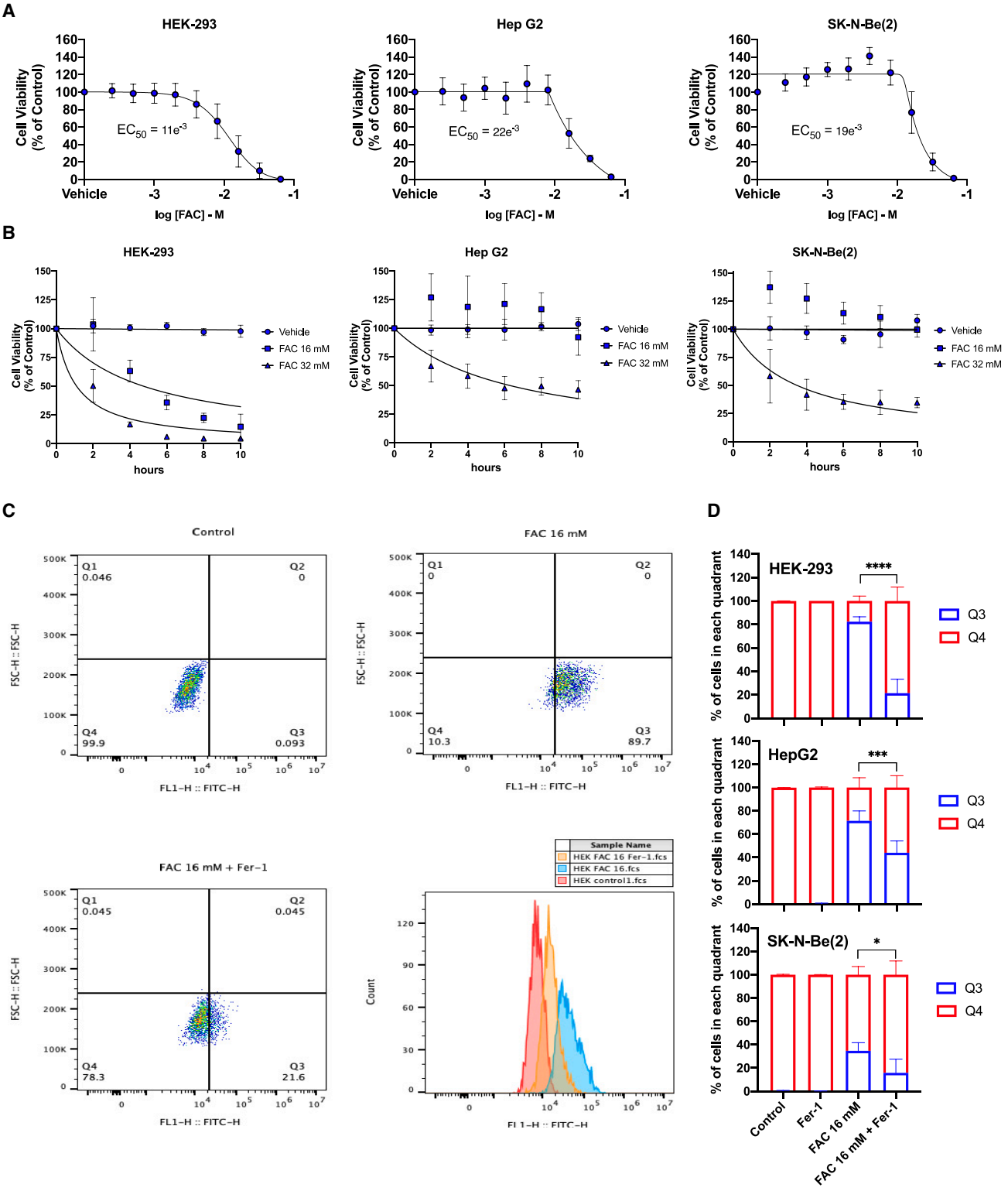

Figure 1. FAC exposure causes early lipid peroxidation and concentration- and time-dependent cytotoxicities in cultured HEK-293, HepG2, and SK-N-Be(2) cells, related to Figure S2

(A and B) Cells were seeded at a density of 2,000 cells/well in 384 well-plates. After 24 h, cells were treated with different ferric ammonium citrate (FAC) concentrations. After 24 h (A) or at different time-points (B), cell viability was evaluated. Data are presented as % of control. Mean ± SD (n = 3).

(legend continued on next page)

Please cite this article in press as: Mann et al., Ferroptosis inhibition by oleic acid mitigates iron-overload-induced injury, Cell Chemical Biology (2023), https://doi.org/10.1016/j.chembiol.2023.10.012

and in the composition and physical properties of membranes, also exhibit regulatory roles in distinct forms of regulated cell death.[28–32] It has been shown that the oxidation of mitochondrial cardiolipin is required for release of cytochrome *c*,[33] a key event contributing to apoptosis.[34] Moreover, some lipids are able to directly interact with the pro-apoptotic protein Bcl-2-associated X protein (Bax), increasing membrane permeabilization and stimulating the subsequent apoptotic dismantling of cells.[35] Concerning necroptosis, a direct interaction between membrane phospholipids and the pore-forming protein mixed lineage kinase domain-like (MLKL) is needed for the execution of this type of regulated cell death.[30–32]

Ferroptosis is critically modulated by lipids. For example, the enzyme acyl-coenzyme A (CoA) synthetase long-chain family member 4 (ACSL4), which has a marked preference for activating polyunsaturated fatty acids (PUFAs) to fatty acyl-CoA (an essential step before incorporation into glycerophospholipids), is required for ferroptotic cell death.[36–38] Transcription factors modulating lipid metabolism, such as peroxisome-proliferator-activated receptors (PPARs), have also been reported to regulate ferroptosis.[39–41] MDM2 and MDMX proteins, which are negative regulators of the tumor suppressor p53, promote ferroptosis in a PPAR-α-dependent manner.[39] On the other hand, increased ferroptosis resistance of pancreatic ductal adenocarcinoma cells has been reported to be a PPAR-γ-dependent event[40] and PPAR-α activation can alleviate ferroptosis in mouse liver.[41]

Recently, it has been shown that monounsaturated fatty acids (MUFAs) provide a ferroptosis-resistant phenotype in cultured cells.[42] Under *in vitro* conditions, the ferroptosis-resistant cellular state induced by exogenous MUFAs is dependent on ACSL3 and characterized by reduced total levels of PUFA-containing phospholipids (PUFA-PLs) and reduced sensitivity to lipid peroxidation.[42] Whether exogenous MUFAs have anti-ferroptotic effects more generally is unclear. Moreover, the potential modulatory effects of MUFAs on iron-overload-mediated damage have not been explored.

Although iron overload is characterized by excess of this metal in the body and causes significant organ toxicity, the molecular mechanisms mediating its toxic effects are not fully understood. Given the central role of iron in ferroptosis, we hypothesized that this recently discovered type of cell death exhibits a significant role in the long-standing clinical problem of iron-overload-mediated damage, which is in line with the already reported role of ferroptosis in iron-overload-mediated multiorgan dysfunction and death among critically ill patients, as well as in an experimental model of acute iron overload in mice.[11] We report herein that ferroptosis is a driving event in *in vitro* and *in vivo* models of iron overload.

Based on the fact that lipids, including those from exogenous sources, display significant roles in modulating regulated cell death,[32] including ferroptosis,[42] we hypothesized that MUFAs, which have been reported to induce a ferroptosis-resistant phenotype *in vitro*,[42] exhibit beneficial effects against iron-overload-mediated damage through their effects on ferroptosis. We found that oleic acid, a MUFA, inhibited iron-overload-mediated damage in cultured mammalian cell lines by inhibiting ferroptosis, and that this event, which was associated to decreased levels of phospholipids containing PUFAs, was blunted by antagonism of PPAR-α, which also decreased the protein expression of the lipid flippase SLC47A1, known to block metabolic vulnerability to ferroptosis.[43] We also found that dietary oleic acid protected against iron-overload-induced damage and mortality in *C. elegans* and that this protection was blunted in animals lacking the nuclear hormone receptor NHR-49, which has homology of function with the mammalian PPAR-α. Dietary oleic acid also inhibited FAC-induced liver lipid peroxidation and damage in a mouse model of iron overload.

RESULTS

Experimental iron overload causes ferroptosis-dependent cytotoxicity *in vitro*

Excess intracellular iron is a primary event leading to organ damage in iron overload patients. To investigate the role of ferroptosis in iron-overload-mediated damage, we first developed an *in vitro* model based on exposure to ferric ammonium citrate (FAC) in cultures of renal (HEK-293), hepatic (Hep G2), and neuronal (SK-N-Be(2)) cell lines. At 24 h after exposure, FAC caused a concentration-dependent decrease in metabolic viability of all three cell lines, with EC_{50} values ranging from 11 to 22 mM (Figure 1A). In time course experiments (up to 10 h) investigating the effects of exposure to fixed concentrations of FAC (16 or 32 mM), a significant time-dependent decrease in cell viability was induced by 32 mM FAC even at initial timepoints, such as 2 h after the start of exposures (Figure 1B). Concerning the exposures to 16 mM FAC for up to 10 h, only HEK-293 cells exhibited decreased viability, including at 4 and 6 h after the start of exposure (Figure 1B). Despite this reduced viability, HEK-293 cells exposed to 16 mM FAC were alive and exhibited normal morphology at 4 and 6 h after the start of exposure (not shown).

We investigated the potential involvement of ferroptosis, apoptosis, and necroptosis in this *in vitro* model of iron overload. Ferrostatin-1 (Fer-1), a specific inhibitor of ferroptosis,[44] significantly protected against FAC-induced cytotoxicity in all cell types (Figures S1A, S1D, and S1G). Z-VAD-FMK, a specific inhibitor of caspases and apoptosis that protected against the cytotoxicity elicited by the BCL-2 inhibitor ABT-199 (Figure S1K), was unable to protect against FAC-induced cytotoxicity (Figures S1B, S1E, and S1H). The combination of necrostatin-1s plus necrosulfonamide, which exhibited significant (even though small) protection against necroptosis (induced by Z-VAD-FMK/TNF-α/LCL-161) (Figure S1L), did not affect FAC-induced cytotoxicity in any tested cell types (Figures S1C, S1F, and S1I). These results indicate that ferroptosis plays a

(C and D) HEK-293, Hep G2, and SK-N-Be(2) cells were seeded at a density of 350,000 cells/well in 6 well-plates. After 24 h, cells were treated with FAC (16 mM) and/or Fer-1 (5 μM). After 6 h, lipid peroxidation was evaluated by Bodipy C11 staining in the flow cytometer. (C) Representative flow cytometer plots of HEK-293 cells. (D) Quantitative analyses of HEK-293, Hep G2, and SK-N-Be(2) cells present in the quadrants 3 and 4 (Q3 and Q4). *$p < 0.05$, ***$p < 0.001$, and ****$p < 0.0001$ by two-way ANOVA followed by Tukey's multiple comparisons test. Mean ± SD (n = 3). Representative flow cytometer plots of Hep G2 and SK-N-Be(2) cells are depicted in Figure S2.

Please cite this article in press as: Mann et al., Ferroptosis inhibition by oleic acid mitigates iron-overload-induced injury, Cell Chemical Biology (2023), https://doi.org/10.1016/j.chembiol.2023.10.012

significant role in *in vitro* models of iron overload, whereas apoptosis and necroptosis are dispensable. Considering the partial protective effect of Fer-1 against FAC-induced cytotoxicity (Figures S1A, S1D, and S1G), the occurrence of yet other types of specific or non-specific cell death cannot be ruled out in our model.

To further explore the involvement of ferroptosis in cell models of iron overload, we investigated the occurrence of lipid reactive oxygen species (ROS) in FAC-exposed cells. During ferroptosis, lipid ROS can be detected using the fluorescent lipid peroxidation sensor C11 BODIPY 581/591.[16] Flow cytometry analyses were performed at 6 h after exposures to 16 mM FAC because of the lack of substantial changes in viability and morphology of the three studied cell lines at this condition. FAC exposures significantly increased lipid ROS accumulation in all cell types (Figures 1C, 1D, S2A, and S2B). Fer-1, which protected against FAC-induced cytotoxicity (Figures S1A, S1D, and S1G), decreased FAC-induced lipid ROS accumulation (Figures 1C, 1D, S2A, and S2B). Taken together, the results from these *in vitro* models indicate that iron overload causes ferroptosis in the three studied cell lines, corroborating previous data on the role of ferroptosis in mediating the cytotoxicity induced by exogenously added iron in cultured cells.[45]

Ferroptosis mediates iron-overload-induced damage/mortality in *C. elegans*

Our findings in these cell line studies prompted further analysis of the role of ferroptosis in an *in vivo* model of iron overload. In wild-type *C. elegans* (N2 strain), FAC exposure caused concentration-dependent mortality at 96 h (Figure 2A), although no significant change in mortality was observed at 48 h, with exception of the highest tested concentration (145 mM) (Figure 2A). Based on these results, we investigated the potential accumulation of lipid ROS at 48 h after exposure to 50 mM FAC. Under such condition (50 mM FAC; 48 h), which preceded the significant effects of FAC toward mortality observed at 96 h, worms exhibited a significant increase in lipid ROS levels (Figures 2B and 2C), suggesting the potential involvement of ferroptosis in iron-overload-induced mortality in *C. elegans*. Notably, increased levels of lipid ROS were particularly detected in intestinal cells (Figure S3), which perform many of the complex functions of the mammalian digestive tract, liver, and fat tissues.[46] To confirm the involvement of ferroptosis in the observed lower survival rate, we investigated the protective effect of the ferroptosis inhibitor Fer-1 against FAC-induced mortality in *C. elegans*. Fer-1 was able to decrease FAC-induced worm mortality (Figure 2D). Notably, butylated hydroxytoluene (BHT), a lipophilic antioxidant that has been reported to inhibit ferroptosis,[47] also inhibited iron-overload-induced mortality in *C. elegans* (Figure 2D). These results indicate that this *in vivo* model of iron overload causes ferroptosis-dependent damage and mortality in *C. elegans.*

Exogenous oleic acid protects against iron-overload-induced cytotoxicity and lipid peroxidation *in vitro*

In cultured cells, exogenous MUFAs inhibit ferroptosis induced by RSL3,[48] erastin2, and ML162.[42] Given the involvement of ferroptosis in our *in vitro* model of iron overload, we hypothesized that exogenous oleic acid, a MUFA, would exhibit protective effects in this context. The effects of four different fatty acids (FAs) (stearic acid [18:0; saturated FA], oleic acid [18:1; MUFA], linoleic acid [18:2; PUFA], and arachidonic acid [20:4; PUFA]) and/or FAC in HEK-293, Hep G2, and SK-N-Be(2) cells are depicted in Figure 3. In the absence of FAC treatment, all the given FAs were toxic at high concentrations (>100 μM), although these effects were cell-type dependent. Addition of oleic acid (up to 100 μM) displayed significant protection against FAC-induced cytotoxicity in HEK-293 (Figure 3A) and Hep G2 cells (Figure 3B), although the magnitude of such protection was dependent FAC concentrations. On the other hand, addition of stearic acid or arachidonic acid made HEK-293 (Figure 3A) and Hep G2 (Figure 3B) cells more susceptible to FAC-mediated cytotoxicity. FAC-mediated toxicity in SK-N-Be(2) was not notably affected by oleic acid treatment (Figure 3C).

Given the anti-ferroptotic effects of oleic acid under *in vitro* conditions[42,48] and the involvement of ferroptosis in the *in vitro* model of iron overload, we hypothesized that the protective effects afforded by oleic acid against iron overload would be related to the mitigation of ferroptosis. To test this hypothesis, we investigated the ability of oleic acid to inhibit iron-overload-induced lipid ROS accumulation (a hallmark of ferroptosis) at 6 h after exposure to 16 mM FAC. Under such conditions (exposure to 16 mM FAC for 6 h), FAC treatment significantly increased lipid ROS accumulation and this was inhibited by oleic acid (Figures 3D and 3E). Given the involvement of ferroptosis in our *in vitro* model, the observed inhibitory effects of oleic acid toward FAC-induced lipid ROS accumulation, and subsequent cytotoxicity emphasize the anti-ferroptotic properties of this MUFA.[42,48]

Oleic acid blocks iron-overload-induced lipid peroxidation and mortality in the *C. elegans*

Given the inhibitory effects of oleic acid on iron-overload-induced ferroptosis in cultured cells (Figure 3), we hypothesized that this MUFA would exhibit analogous effects *in vivo*. This hypothesis was also based on the previously reported beneficial effects of oleic acid in *C. elegans* models of ferroptosis in germline cells.[49,50] To test this hypothesis, wild-type (N2 strain) *C. elegans* were treated from larval stage 1 (L1) with dietary oleic acid and challenged at stage L4 with 50 or 100 mM FAC, which is known to induce ferroptosis-dependent mortality in *C. elegans* (Figure 2). Parallel groups were treated with stearic or linoleic acids for comparison. As previously shown (Figure 2), experimental iron overload (50 and 100 mM FAC) induced significant mortality in worms at 96 h (Figure 4A). Notably, dietary oleic acid significantly inhibited iron-overload-induced mortality; this effect was observed at both FAC concentrations (50 and 100 mM). Stearic or linoleic acids exhibited no relevant protective effects (Figure 4A).

Based on the pivotal role of lipid peroxidation in ferroptosis,[16] we investigated the effects of dietary FAs (oleic, stearic, and linoleic) on the accumulation of lipid ROS at 48 h after 50 mM FAC exposure, a condition characterized by lack of changes in the mortality rate (Figure 4A). As previously observed (Figure 2B), a significant increase in lipid ROS was detected in worms exposed to 50 mM FAC for 48 h (Figures 4B and 4C). Although stearic and linoleic acids did not reduce FAC-induced increase in lipid ROS, dietary oleic acid significantly decreased iron-overload-induced lipid peroxidation in *C. elegans* (Figures 4B and 4C), indicating

Please cite this article in press as: Mann et al., Ferroptosis inhibition by oleic acid mitigates iron-overload-induced injury, Cell Chemical Biology (2023), https://doi.org/10.1016/j.chembiol.2023.10.012

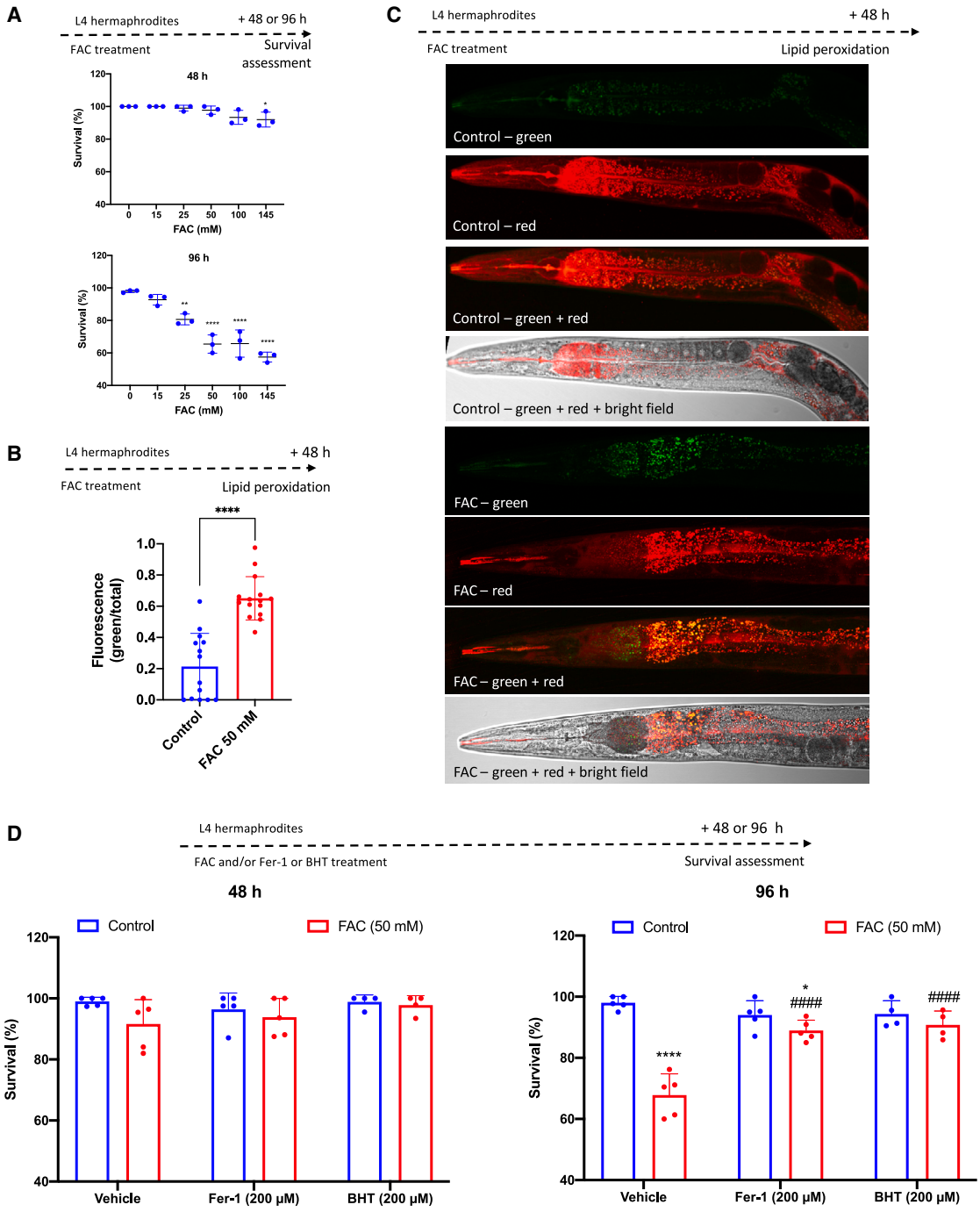

Figure 2. Experimental iron overload causes ferroptosis-dependent damage and mortality in *C. elegans*

(A) Wild-type (N2 strain) L4 worms were exposed to different concentrations of ferric ammonium citrate (FAC) during 48 or 96 h. Survival rate is presented as % the initial number of alive animals (~25/experiment/group). Data are represented as mean ± SD (N = 3). Significant differences were analyzed by one-way ANOVA followed by Dunnett's test. *p < 0.05, **p < 0.01, ****p < 0.0001 compared to control.

(B and C) Wild-type (N2 strain) L4 worms were exposed to vehicle (control) or 50 mM FAC during 48 h. (B) Lipid peroxidation (BODIPY-C11 staining) is presented as fluorescence [green/(green + red)]. ****p < 0.0001 by Student test. N = 15 worms per group (derived from 3 independent experiments). (C) Representative confocal microscopy images of red and/or green BODIPY-C11 fluorescence in control and FAC-exposed worms.

(D) Wild-type (N2 strain) L4 worms were exposed to 50 mM FAC and/or 200 µM Fer-1 or 200 µM BHT for 48 or 96 h. Survival rate is presented as % the initial number of live animals (~25/experiment/group). Data are represented as mean ± SD (N = 5). Significant differences were analyzed by two-way ANOVA followed by Tukey's test. *p < 0.05, ****p < 0.0001 compared to control. ####p < 0.0001 compared to worms exposed only to 50 mM FAC.

Please cite this article in press as: Mann et al., Ferroptosis inhibition by oleic acid mitigates iron-overload-induced injury, Cell Chemical Biology (2023), https://doi.org/10.1016/j.chembiol.2023.10.012

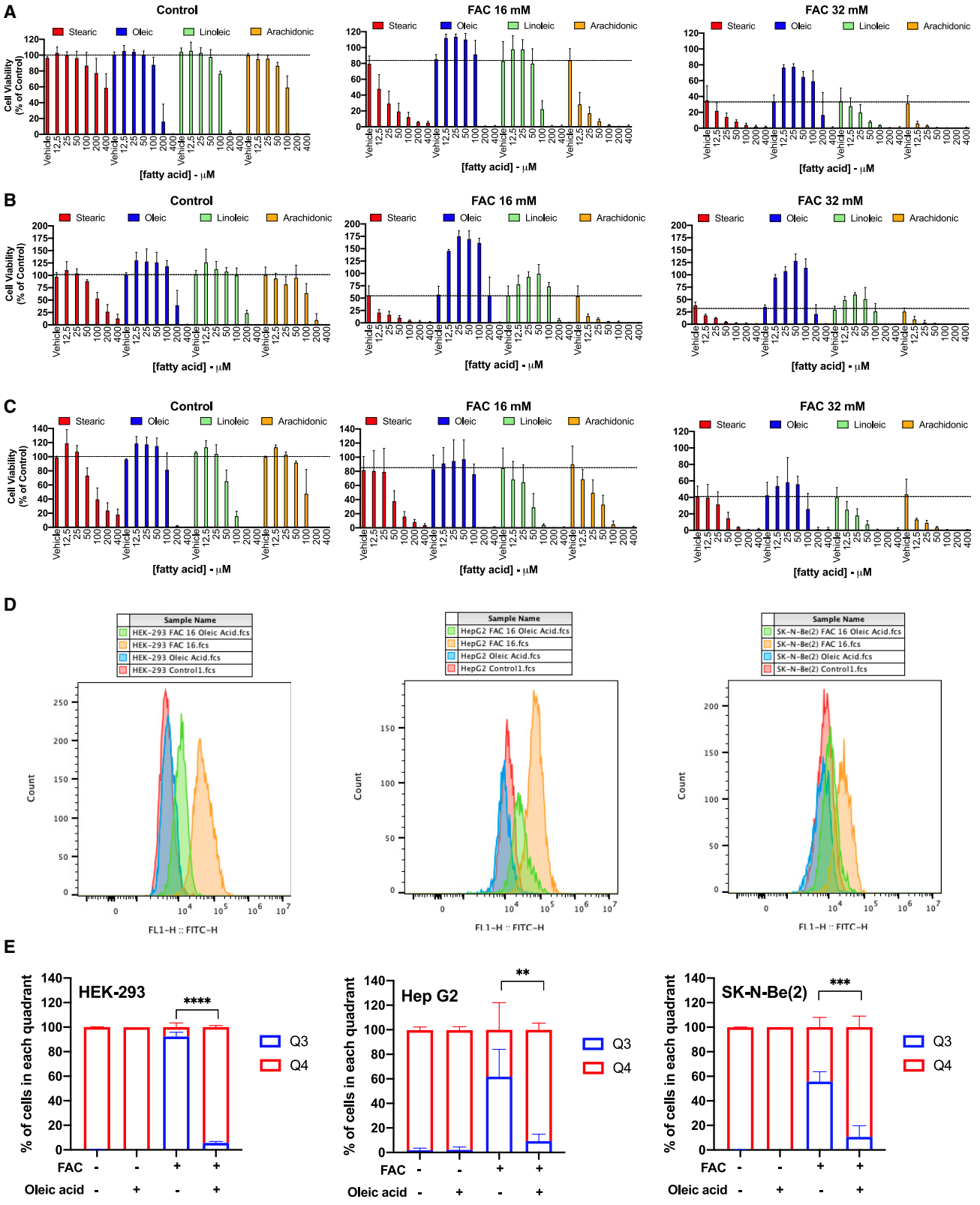

Figure 3. Oleic acid inhibits FAC-induced cytotoxicity and lipid peroxidation in cells

(A–C) HEK-293 (A), Hep G2 (B), and SK-N-Be(2) (C) cells were seeded at a density of 2,000 cells/well in 384 well-plates. After 90 min, cells were treated with different concentrations (12.5–400 μM) of stearic, oleic, linoleic, and arachidonic acids. After 24 h, cells were treated with FAC (0, 16 mM and 32 mM) and, after

(legend continued on next page)

Please cite this article in press as: Mann et al., Ferroptosis inhibition by oleic acid mitigates iron-overload-induced injury, Cell Chemical Biology (2023), https://doi.org/10.1016/j.chembiol.2023.10.012

that the protective effects of this MUFA against iron-overload-induced mortality is due to its anti-ferroptotic properties. Given the involvement of ferroptosis in the *in vivo* model of iron overload (Figure 2), the observed inhibitory effects of dietary oleic acid toward FAC-induced lipid ROS accumulation and subsequent mortality in *C. elegans* highlight the *in vivo* anti-ferroptotic properties of this MUFA.

Oleic acid treatment modifies lipid composition, but causes minor effects in gene and protein expression in cultured cells

Under *in vitro* conditions, MUFAs may inhibit ferroptosis by promoting the displacement of PUFAs from plasma membrane phospholipids.[42] To investigate mechanisms mediating the protective effects of oleic acid against iron-overload-mediated ferroptosis, we performed lipidomic analyses of HEK-293 cells treated with 50 μM oleic acid and/or 16 mM FAC (Figure 5). Although FAC treatment caused minor effects on cellular lipid composition, oleic acid treatment triggered a major change in cellular lipid composition, which was characterized by decreased levels of PUFAs-containing phospholipids (i.e., PE 16:0_20:4; PE 16:0_22:6; PG 18:1_22:4; PG 18:1_22:5), corroborating the ferroptosis-resistant phenotype elicited by oleic acid, as well as decreased levels of ether-linked phospholipids (i.e., PE O-16:0_20:5; PE O-16:1_16:0; PE O-16:1_22:6; PE O-18:0_18:3; PE O-18:0_20:4; PE O-18:0_20:5; PE O-18:1_22:4; PE O-18:1_22:5; PE O-20:0_20:4; PE O-32:0; PE O-36:2; PE O-38:4; PE O-38:6) (Figure 5).

Considering the role of lipids (including FAs) in cell signaling[51] and gene regulation,[52,53] we also investigated whether the anti-ferroptotic properties of oleic acid could be related to changes in the expression of genes and/or proteins known to modulate ferroptosis. Particularly, we investigated whether 50 μM oleic acid, which protected HEK-293 and Hep G2 cells against iron-overload-induced ferroptosis (Figure 3), could modulate the expression of the anti-ferroptotic enzyme glutathione peroxidase 4 (GPx4), which detoxifies lipid peroxides and is considered a primary enzyme preventing ferroptosis,[47,54] as well as ACSL4, which seems to be essential for ferroptosis triggered by the direct inhibition of GPX4.[55] We also evaluated the expression of ferroptosis suppressor protein 1 (FSP1), a CoQ oxidoreductase that acts parallel to GPx4 to inhibit ferroptosis,[56] and xCT, whose activity allows for the proper uptake of cystine (a GSH precursor) and detoxification of lipid peroxide through the GPx4 pathway. Even though there were clear differences in basal expression of these proteins between the three evaluated cell types, no significant effects of oleic acid and/or FAC were observed (Figure S4), suggesting that alterations in the levels of the investigated proteins are likely not involved in the anti-ferroptotic and cytoprotective effects of oleic acid or the effects of FAC. However, the potential occurrence of post-translational and/or functional regulation of these proteins cannot be ruled out.

To further investigate mechanisms mediating the protective effects of oleic acid against iron-overload-mediated ferroptosis, we performed transcriptomic (Figure S5) and proteomic (Figure S6) analyses of HEK-293 cells treated with 50 μM oleic acid and/or 16 mM FAC. Transcriptomic analyses indicated a significant effect of FAC treatment on the expression of genes involved in iron and cholesterol metabolism (i.e., TRFC, INSIG1, and MSMO1), but oleic acid was unable to reverse these effects of FAC (Figure S5). In agreement, the observed changes in protein expression after FAC treatment (i.e., IREB2, APLP2, and TMEM59) were not suppressed by oleic acid (Figure S6). In short, oleic acid treatment caused minor effects in both transcriptomic and proteomic cellular profile, suggesting that the protective effect of oleic acid on FAC toxicity does not depend on transcriptional or proteomic changes.

Oleic acid-mediated protection against iron overload-damage in HEK-293 cells is attenuated by the PPAR-α antagonist GW6471

Based on recent studies reporting the involvement of PPARs in ferroptosis,[39–41,57] we wonder if PPARs could play significant role(s) in the observed protective effects elicited by oleic acid. Thus, we further investigated the potential modulatory effects of PPAR antagonists (GW 6471, PPAR-α antagonist, and T0070907, PPAR-γ antagonist) on oleic-acid-mediated protection against iron-overload-mediated cytotoxicity. The PPAR-γ antagonist T0070907 exhibited no significant effects (Figure 6A), but the PPAR-α antagonist GW6471 significantly decreased oleic-acid-induced protection against FAC exposure in HEK-293 and Hep G2 cells (Figure 6B). This result indicates that the anti-ferroptotic effects of this MUFA are decreased, at least partially, upon PPAR-α antagonism.

Considering the existence of PPAR-responsive elements in the promoter region of the gene encoding ACSL3,[58] as well as the crucial role of this protein in modulating the anti-ferroptotic effects of oleic acid,[42] we investigated if the PPAR-α antagonist GW6471, which mitigated the protective effects of oleic acid against FAC (Figure 6B), could affect ASCL3 protein expression. Western blotting analyses showed no significant effects of GW6471 on ASCL3 protein levels in HEK-293 cells (Figure 6C), suggesting that alterations in the levels of ASCL3 are likely not involved in the inhibitory effect of GW6471 toward the cytoprotective effects of oleic acid. Considering the recent evidence that the lipid flippase solute carrier family 47 member 1 (SLC47A1) inhibits ferroptosis, we further tested if GW6471 could affect SLC47A1 protein expression. The motivation for such experiments was based on the fact that SLC47A1, whose basal expression was reported to be modulated by PPAR-α,[43] blocks the metabolic vulnerability to ferroptosis through a

additional 24 h, cell viability was evaluated. Data are presented as % of vehicle-treated cells. Mean ± SD (n = 3). Dashed lines indicate the average of cell viability without fatty acids addition: just vehicle (0.5% ethanol) and FAC (0, 16, or 32 mM). (D–E) HEK-293, Hep G2, and SK-N-Be(2) cells were seeded at a density of 350,000 cells/well in 6 well-plates. After 90 min, cells were treated with vehicle or 50 μM oleic acid. After 24 h, cells were treated with vehicle or 16 mM FAC and, after 6 h, lipid peroxidation was evaluated by Bodipy C11 staining in the flow cytometer.

(D) Representative plots of HEK-293, Hep G2, and SK-N-Be(2) cells.

(E) Quantitative analyses of HEK-293, Hep G2, and SK-N-Be(2) cells present in the quadrants 3 and 4 (Q3 and Q4). **$p < 0.01$, ***$p < 0.001$, and ****$p < 0.0001$ by two-way ANOVA followed by Tukey's multiple comparisons test.

Please cite this article in press as: Mann et al., Ferroptosis inhibition by oleic acid mitigates iron-overload-induced injury, Cell Chemical Biology (2023), https://doi.org/10.1016/j.chembiol.2023.10.012

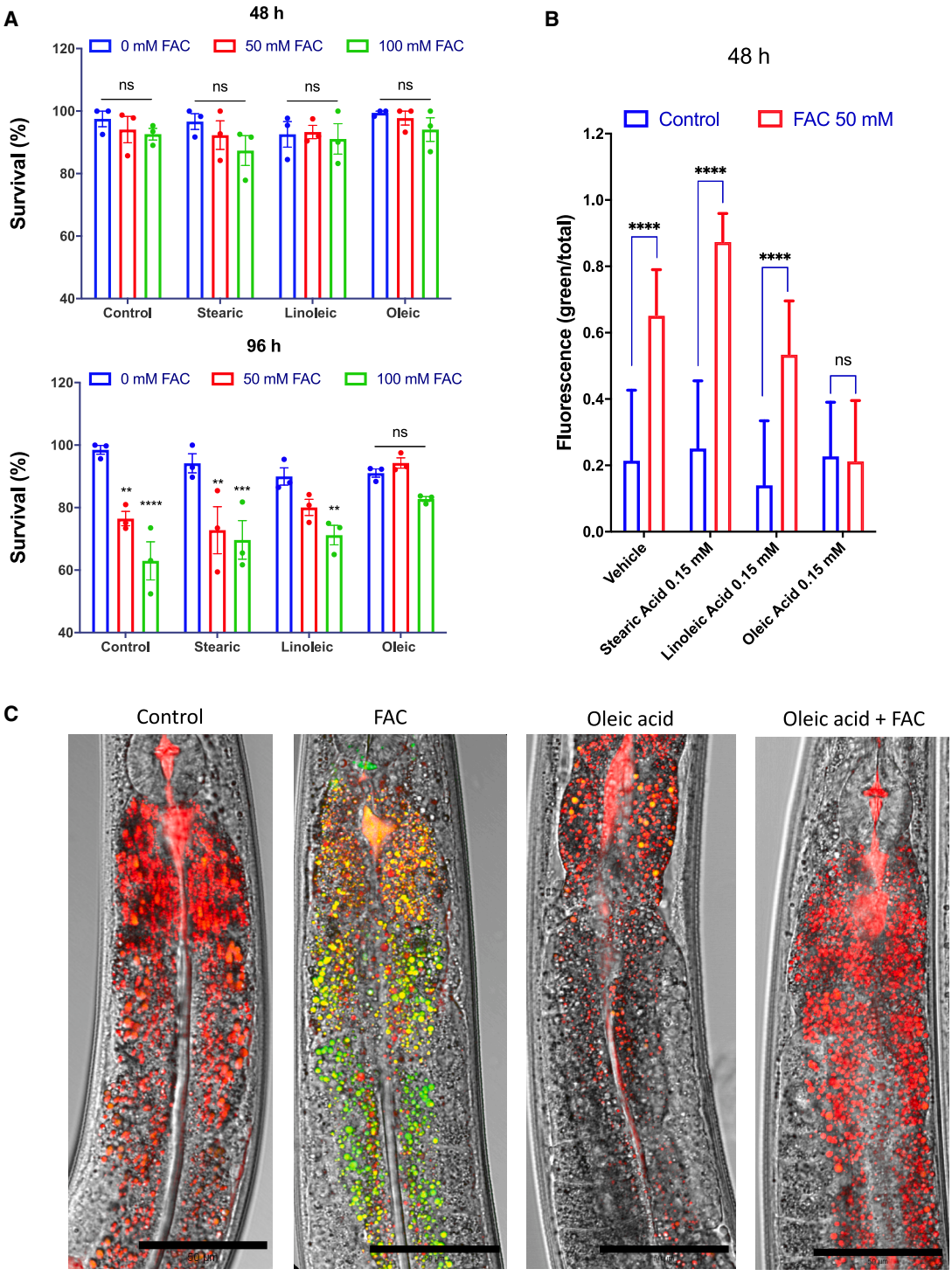

Figure 4. Oleic acid prevents FAC-induced mortality and lipid peroxidation in *C. elegans*

(A) Wild-type (N2 strain) worms were exposed to different 0.15 mM of stearic, linoleic, or oleic acid from L1. At the L4 stage, worms were exposed to 50 or 100 mM FAC during 48 or 96 h. Survival rate is presented as % the initial number of live animals (~25/experiment/group). Data are represented as mean ± SD (N = 3). $^{**}p < 0.01$, $^{****}p < 0.0001$ compared to the respective control after two-way ANOVA followed by Tukey's multiple comparisons test.

(B and C) Wild-type (N2 strain) worms were exposed to vehicle or 0.15 mM of stearic, linoleic or oleic acid from L1. At the L4 stage, worms were exposed to 50 mM FAC during 48. (B) Lipid peroxidation (BODIPY-C11 staining) is presented as fluorescence [green/(green + red)]. $^{****}p < 0.0001$ by one-way ANOVA. N = 15 worms per group (derived from 3 independent experiments). ns = non-significant. (C) Representative confocal microscopy images of bright field + red and green BODIPY-C11 fluorescences from control, FAC (50 mM), oleic acid (0.15 mM), and FAC (50 mM) + oleic acid (0.15 mM)-exposed worms (48 h after FAC exposure). Scale bar: 50 μm.

Please cite this article in press as: Mann et al., Ferroptosis inhibition by oleic acid mitigates iron-overload-induced injury, Cell Chemical Biology (2023), https://doi.org/10.1016/j.chembiol.2023.10.012

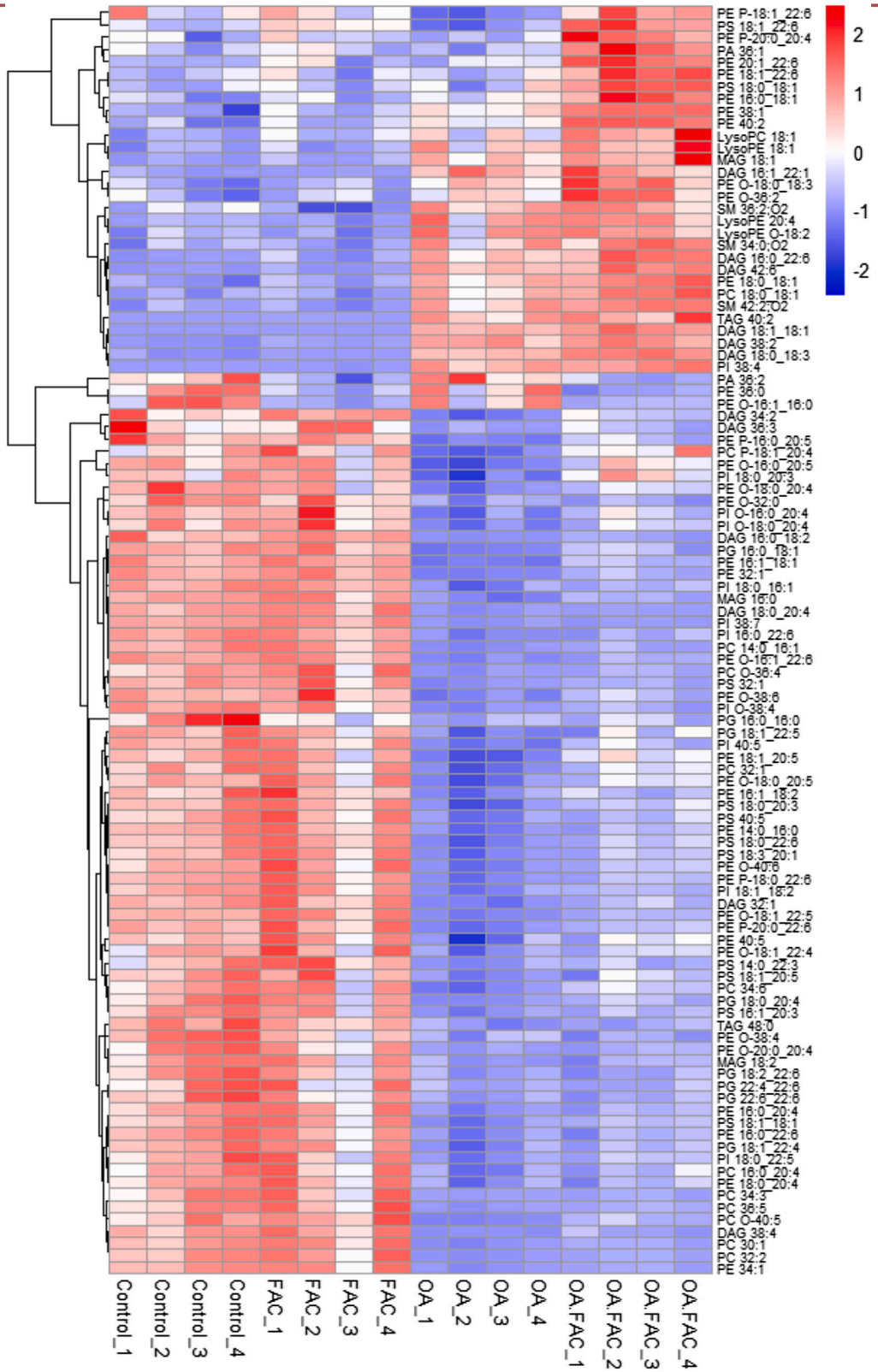

Figure 5. Oleic acid decreases PUFA-containing and ether-related phospholipids

Heatmap of significantly changed lipid species (one-way ANOVA; FDR-corrected $p < 0.05$; $n = 4$ biologically independent samples) measured in duplicates using UPLC–MS. Each row represents z-score-normalized intensities of the detected lipid species. Each column represents a sample. The relative abundance of each

(legend continued on next page)

Please cite this article in press as: Mann et al., Ferroptosis inhibition by oleic acid mitigates iron-overload-induced injury, Cell Chemical Biology (2023), https://doi.org/10.1016/j.chembiol.2023.10.012

cellular lipid reprogramming profile similar to that induced by oleic acid (decreasing PUFA-containing phospholipids). Notably, we observed that the PPAR-α antagonist GW6471, which mitigated the protective effects of oleic acid against FAC, was able to decrease the protein expression of SLC47A1 (Figure 6D). GW6471 also inhibited the protective effects of oleic acid against the cytotoxic effects of the canonical ferroptosis inducer RSL3 (Figure 6E).

Because *C. elegans* has no direct PPAR or orthologues, the investigation of direct relationships between PPAR-α and oleic-acid-induced anti-ferroptotic effects in the nematode model is not feasible. Despite this limitation, NHR-49 has been reported as a homologue of function of the mammalian PPAR-α in *C. elegans*.[59,60] Therefore, we investigated the protective effects of dietary oleic acid against iron-overload-induced mortality in *C. elegans* knocked out for NHR-49 (the STE68 strain: loss of function of nhr-49(nr2041)[59]). Remarkably, the protective effect of dietary oleic acid against iron-overload-induced mortality was blunted in worms lacking the nuclear hormone receptor NHR-49 (Figure S7). Moreover, 50 and 100 mM FAC exposure for 144 h caused a higher mortality rate in NHR-49 animals (a survival rate near to 50%) compared to the wild-type N2 strain (survival rate near to 75%) (Figure S7). This result seems to be in line with the fact that NHR-49 stimulates the expression of FA D9-desaturase genes, facilitating the conversion of saturated FAs to MUFAs,[59] and consequently, NHR-49 mutant animals are lower in monounsaturated fat, which would explain the higher susceptibility to ferroptosis. Such idea is in line with the fact that NHR-49 mutants are highly sensitive to DGLA-induced ferroptosis.[61] Although *C. elegans* has no direct PPARs or orthologues, NHR-49 represents a functional homologue of the mammalian PPAR-α, and the present data on the lack of significant anti-ferroptotic effects of oleic acid in NHR-49 animals (but not in wild-type animals) represent an intriguing research topic that deserves further attention.

Oleic acid protects against iron-overload-induced liver lipid peroxidation and damage in mice

In order to investigate the potential antiferroptotic properties of oleic acid in a more complex mammalian scenario, a mouse-based assay was performed; it was based on a previously reported rodent model of iron-overload-induced damage, which detected ferroptosis as a key event leading to multiorgan dysfunction and death in mice acutely exposed to Fe.[11] Considering the critical role of liver in iron overload,[13] we investigated liver lipid peroxidation (a driver of ferroptosis) and the serum activity of alanine transaminase (ALT), a peripheral marker of liver damage. The serum activity of lactate dehydrogenase (LDH), a general marker of organ damage, was also evaluated.

At 4 h after FAC administration (120 mg/kg, i.p.), mice exhibited a significant increase in liver lipid peroxidation, as well as increased activities of serum ALT and LDH (Figure 7). Dietary pre-treatment with oleic acid (600 mg/kg/day, *per os*, during 10 days prior FAC exposure) significantly inhibited iron-overload-induced liver lipid peroxidation and increase of serum ALT and LDH activities (Figure 7), pointing to anti-ferroptotic effects of oleic acid in a mammalian (rodent) model.

DISCUSSION

Here, we report that ferroptosis occurs in the context of iron-overload-mediated damage under *in vitro* (cultured cells) and *in vivo* (*C. elegans* and mice) conditions and that exogenously added oleic acid protects against such damage in both scenarios by suppressing ferroptosis. It has been reported that free intracellular iron can boost lipid peroxidation by catalyzing the production of hydroxyl radicals in a Fenton-chemistry-dependent manner.[62] This pivotal role of iron in propelling lipid peroxidation, which represents a driver event in ferroptosis,[16,63] prompted us to hypothesize that ferroptosis mediates iron-overload injury. The increased lipid ROS accumulation observed in cultured cells subjected to iron overload (Figures 1C and 1D) represents initial evidence supporting the occurrence ferroptosis in *in vitro* models. Notably, treatment of cells with the anti-ferroptotic agent Fer-1 not only inhibited lipid ROS accumulation at early periods, but also protected against cell cytotoxicity induced by iron overload at latter time-points, reinforcing the idea that ferroptosis takes place in experimental iron overload injury *in vitro*.

The observed increased lipid ROS accumulation at early periods in *C. elegans* and the significant effects of Fer-1 and BHT in mitigating FAC-induced mortality in worms point to a contribution of ferroptosis to iron-overload injury under *in vivo* conditions, thus highlighting the relevance of this phenomenon in more complex biological scenarios. Even though the presented results are the first to report a significant relationship between dietary iron exposure and ferroptosis in *C. elegans*, it is important to mention that this type of cell death has been reported in this model after changes in iron levels due to aging and glutathione depletion,[64] as well as dietary exposure to the omega-6 PUFA dihomo-gamma-linolenic acid (DGLA; 20:3n-6).[49,65,66] Of note, dietary exposure to DGLA induces sterility in young adult *C. elegans* due to the death of germ cells, oocytes and sperm, while somatic cells remained unaffected.[49] On the other hand, the acute depletion of glutathione induced by diethyl maleate (DEM) in 4-day-old adult worms caused ferroptosis particularly in intestinal cells, which was related to a progressive degeneration contributing to frailty phenotype and organismal death.[64]

In the present study, iron overload-induced ferroptosis at larval stage 4 (L4) caused lipid peroxidation of intestinal cells prior to organismal death (Figure S3). Considering that the *C. elegans* intestine fulfills many of the complex functions of the mammalian digestive tract, liver, and fat tissues, as well as displays vital roles in pathogen defense, immunity, and longevity,[46] it is reasonable to suppose that the increased

lipid is color-coded, with red indicating high signal intensity and blue indicating low signal intensity. DAG, diacylglycerol; LysoPC, lysophosphatidylcholine; LysoPE, lysophosphatidylethanolamine; MAG, monoacylglycerol; PA, phosphatidic acid; PC, phosphatidylcholine; PC P, plasmalogen PC; PE, phosphatidylethanolamine; PE O, ether-linked PE; PE P, plasmalogen PE; PG, phosphatidylglycerol; PI, phosphatidylinositol; PS, phosphatidylserine; SM, sphingomyelin; TAG, triacylglycerol. Lipids are annotated based on their fatty acyl compositions (for example, LysoPC 18:1 has 18 carbons and 1 double bond) or as the sum of their total number of carbons and double bonds (for example, DAG 38:4 has a total of 38 carbons and 4 double bonds).

Please cite this article in press as: Mann et al., Ferroptosis inhibition by oleic acid mitigates iron-overload-induced injury, Cell Chemical Biology (2023), https://doi.org/10.1016/j.chembiol.2023.10.012

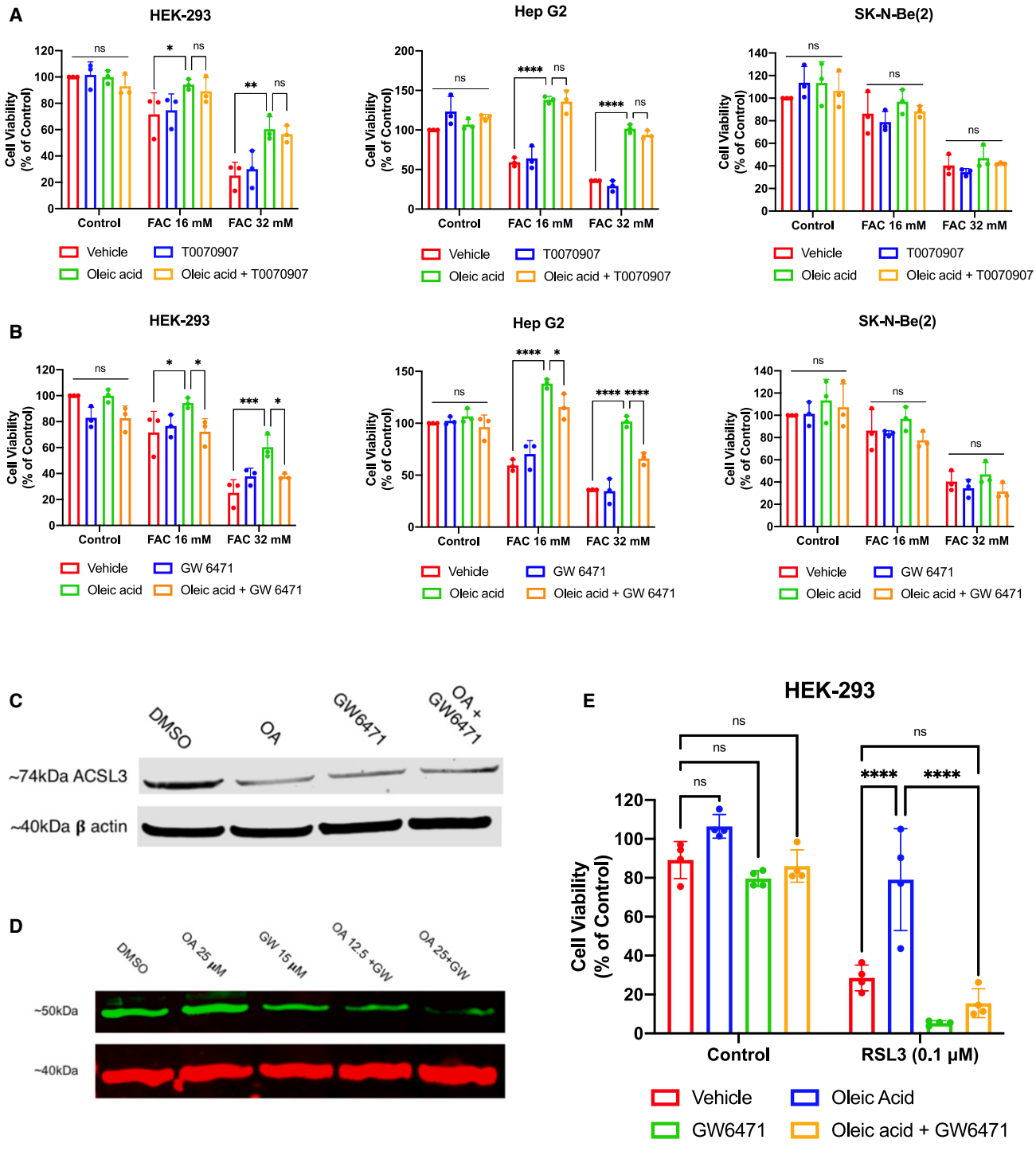

Figure 6. Inhibition of PPAR-α activity decreases the antiferroptotic effects of oleic acid and SLC47A1 protein expression

(A and B) HEK-293, Hep G2, and SK-N-Be(2) cells were seeded at a density of 2,000 cells/well in 384 well-plates. After 90 min, cells were treated with vehicle or 50 μM oleic acid. After 24 h, cells were treated with FAC (0, 16 mM or 32 mM) and/or (A) 10 μM T0070907 (PPAR-γ antagonist) or (B) 10 μM GW 6471 (PPAR-α antagonist). After additional 24 h, cell viability was evaluated. Data are presented as % of control. Mean ± SD (n = 3). *p < 0.05, ***p < 0.001, and ****p < 0.0001 by two-way ANOVA followed by Tukey's multiple comparisons test. ns = non-significant.

(C) ACSL3 protein levels: HEK-293 cells were seeded at a density of $1x10^6$ cells/well in 100 mm dishes. After 90 min, cells were treated with vehicle or 25 μM oleic acid (OA). After 24 h, cells were treated with vehicle (DMSO) or 15 μM GW6471. After 24 h, samples were collected for western blotting analyses.

(legend continued on next page)

Please cite this article in press as: Mann et al., Ferroptosis inhibition by oleic acid mitigates iron-overload-induced injury, Cell Chemical Biology (2023), https://doi.org/10.1016/j.chembiol.2023.10.012

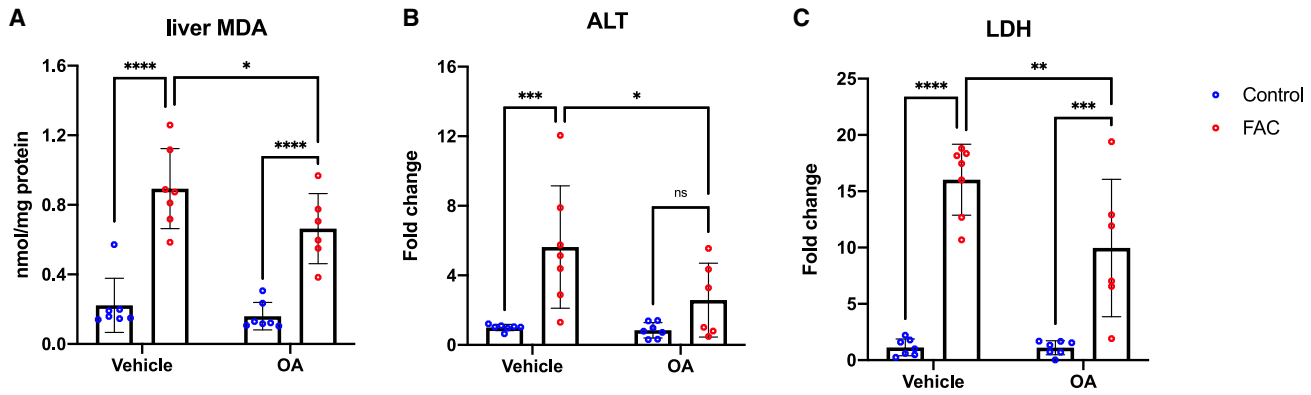

Figure 7. Oleic acid pre-treatment inhibits iron-overload-induced liver lipid peroxidation and damage in mice

Swiss male mice were pretreated with vehicle or oleic acid (600 mg/kg/day; oral route) for 10 days. Thereafter, mice were treated with a single i.p. injection of FAC (120 mg/kg) and euthanized at 4 h after FAC treatment.

(A) Liver malondialdehyde (MDA), serum (B) AST and (C) LDH are presented as mean ± SD (n = 6–7 per group). *p < 0.05, **p < 0.01, ***p < 0.001, and ****p < 0.0001 by two-way ANOVA. ns = non-significant.

mortality observed in FAC-exposed *C. elegans* results, at least partially, from intestinal cells' lipid peroxidation and ferroptosis.

Cultured cells treated with exogenous MUFAs exhibit a resistant phenotype against ferroptosis induced by RSL3,[48] erastin2, and ML 162.[42] MUFA-induced resistance against ferroptosis is dependent of ACSL3 and characterized by reduced total levels of PUFA-containing phospholipids.[42] Here, we observed that oleic acid, a MUFA, protected cultured cells against iron-overload-induced damage *in vitro* (Figure 3), which we found to be due to ferroptosis (Figures 1, S1, and S2). The observed decrease in FAC-mediated lipid ROS accumulation (Figures 3D and 3E) and lower levels of PUFA-containing phospholipids (Figure 5) in oleic acid-treated cells are in agreement with previous data,[42] which indicate that oleic acid would be competing for PUFAs in being incorporated into phospholipids.

Furthermore, lipidomics data in *C. elegans* have shown that the relative levels of some C20 PUFAs, such as DGLA and arachidonic acid, were lowered in oleic-acid-treated worms,[49] consistent with the notion that dietary oleic acid displaces PUFAs from membranes. This competition between different types of FAs for incorporation into phospholipids, which is in agreement with the higher levels of 18:1-containing phospholipids in oleic-acid-treated HEK-293 cells compared to controls (i.e., LysoPC; LysoPE; PC and PE) (Figure 5), could lead one to posit that saturated FAs are not good substrates for such competing processes. This hypothesis is supported by the lack of protective effect of stearic acid against iron overload *in vitro* (Figure 3).

Notably, oleic acid caused a significant decrease in the levels of ether-linked phospholipids, mainly phosphatidylethanolamines (Figure 5). The role of ether-linked lipids in ferroptosis represents a complex matter and seems to depend on the initial pro-ferroptotic trigger. Indeed, although ether lipids were reported to protect cells from ferroptosis induced by dihomo-gamma-linolenic acid (20:3n-6),[49,65] some lines of evidence point to pro-ferroptotic effects of ether lipids.[67,68] Despite the apparent negative relationship between levels of ether-linked phospholipids and the ferroptosis-resistant phenotype, further research is needed to explore whether ether-linked phospholipids exhibit causal pro-ferroptotic roles in iron overload.

The protective effects of oleic acid against FAC-mediated damage in cultured cells, which reinforce the involvement of ferroptosis during iron overload *in vitro*, were validated by results in a *C. elegans* model of iron overload. These results, which point to the possibility of reducing iron-overload-mediated damage through therapeutic/nutritional strategies that inhibit ferroptosis, were corroborated in a mouse model of iron overload (Figure 7), highlighting the potential clinical relevance of these findings to mammals. Available treatments for iron-overload patients are based only on strategies to decrease iron levels, such as iron chelation and phlebotomy. Dietary incorporation of oleic acid thus represents a new therapeutic approach to treating iron overload.

Based on recent studies reporting the involvement of PPARs in ferroptosis,[39–41,57] we wondered if PPARs could play significant role(s) in the observed protective effects elicited by oleic acid. We found that antagonizing PPAR-α with GW6471 significantly decreased oleic-acid-induced protection against FAC exposure in cultured cells (Figure 6B). Notably, we observed that the PPAR-α antagonist GW6471 was also able to decrease protein expression of the flippase SLC47A1 (Figure 6D), a PPAR-α downstream target capable of blocking metabolic vulnerability to ferroptosis through a cellular lipid reprogramming.[43]

(D) SLC47A1 protein levels: HEK-293 cells were seeded at a density of $1x10^6$ cells/well in 100 mm dishes. After 90 min, cells were treated with vehicle, 12.5 or 25 μM oleic acid (OA). After 24 h, cells were treated with vehicle or 15 μM GW6471 (GW). After 24 h, samples were collected for western blotting analyses. The image is a representative of 3 separate blots with similar results. 50 kDa (green) = SLC47A1; 40 kDa (red) = beta-actin.

(E) HEK-293 cells were plated at 10,000 cells per well in white 96-well plates. After 90 min, cells were treated with vehicle or 12.5 μM oleic acid. After 24 h, cells were treated with 100 nM RSL3 and/or 10 μM GW6471 (PPAR-α antagonist). After additional 24 h, cell viability was evaluated. Data are presented as % of control. Mean ± SD (n = 4). ****p < 0.0001 by two-way ANOVA followed by Tukey's multiple comparisons test. ns = non-significant.

Please cite this article in press as: Mann et al., Ferroptosis inhibition by oleic acid mitigates iron-overload-induced injury, Cell Chemical Biology (2023), https://doi.org/10.1016/j.chembiol.2023.10.012

Considering that in *C. elegans* the nuclear hormone receptor NHR-49 has homology of function with the mammalian PPAR-α,[59] we tested the effects of oleic acid against iron overload-mediated injury in worms knocked out for NHR-49. The inhibition of the protective effect of oleic acid against iron-overload-induced mortality in worms lacking the nuclear hormone receptor NHR-49 could lead one to posit that the anti-ferroptotic effects of this MUFA in *C. elegans* depend on NHR-49 activity, implying that an oleic acid signal is acting through NHR-49 transcriptional responses to ultimately protect against ferroptosis. However, an alternative and more likely hypothesis to explain the loss of oleic-acid-mediated protection against iron overload in nhr-49 mutants is that the metabolic abnormalities resulting from NHR-49 knockout are so great that the usually beneficial roles of oleic acid are not enough to overcome all the other defects induced by NHR-49 knockout that make the worms more susceptible to ferroptosis. This hypothesis is based on the fact that nhr-49 mutants were more sensitive to FAC-induced mortality (Figure S7) and have several lipid homeostasis defects (nhr-49 mutants are sick animals with reduced lifespan, higher fat content and impaired lipolysis).[59] Even though these results clearly indicate that the beneficial effects of oleic acid were lower upon PPAR-α antagonism (cells) or NHR-49 knockout (*C. elegans*), additional research is needed to provide mechanistic insights into the relationship between these nuclear receptors and the anti-ferroptotic effects of oleic acid.

Taken together, these results point to ferroptosis as a driver of iron-overload-mediated damage and indicate that oleic acid inhibits iron-overload-induced ferroptotic damage in cultured cells, *Caenorhabditis elegans* and mice. The results suggest that dietary treatment with oleic acid might represent a useful therapeutic strategy to mitigating organ damage observed in iron overload individuals, although concomitant use with PPAR-α antagonists should likely be avoided.

Limitations of the study

Our findings indicate that the protective effects of oleic acid against iron overload-mediated injury are decreased upon PPAR-α antagonism or NHR-49 knockout. Although these results suggest potential modulatory effects of PPAR-α/NHR-49 in oleic acid-mediated protection, it remains to be determined the mechanisms of the relationship between these nuclear receptors and the anti-ferroptotic effects of oleic acid. Furthermore, the observed protective effects of oleic acid against iron overload-induced liver injury in mice were derived from an acute iron overload model. Considering that human iron overload is a chronic condition, it will be important to determine if this MUFA displays beneficial antiferroptotic effects in a chronic (long-term) mouse model of iron overload.

SIGNIFICANCE

Iron overload disorders represent an important class of human diseases characterized by excess iron in the body, leading to substantial toxicity to diverse organs. The molecular mechanisms mediating iron-overload-induced toxicity are not yet understood and current treatments are based on strategies to decrease iron levels, such as iron chelation and phlebotomy. Here, we found that ferroptosis is a driving event in iron-overload mediated damage *in vitro* (cultured cells) and *in vivo* (*C. elegans* and mice). We also found that exogenously added oleic acid, a MUFA, protected against iron-overload mediated damage by inhibiting ferroptosis in cells and worms. Moreover, the anti-ferroptotic effects of oleic acid in cultured cells were related to a cellular lipidomic reprogramming. These results point to the possibility of reducing iron-overload-mediated damage through therapeutic, nutritional strategies that inhibit ferroptosis; dietary incorporation of oleic acid might represent a new therapeutic approach to treating iron-overload.

STAR★METHODS

Detailed methods are provided in the online version of this paper and include the following:

- KEY RESOURCES TABLE
- RESOURCE AVAILABILITY
  - Lead contact
  - Materials availability
  - Data and code availability
- EXPERIMENTAL MODEL AND STUDY PARTICIPANT DETAILS
  - Cell lines and culture conditions
  - *C. elegans* strains and conditions
  - Mice
- METHOD DETAILS
  - Cell viability assessment
  - Lipid ROS assay using flow cytometer
  - Western blot analysis
  - Lipidomic analyses
  - LC conditions
  - MS conditions
  - Lipidomic data preprocessing and analysis
  - RNA sequencing and data analysis
  - Global quantitative proteomics analysis
  - *C. elegans* treatments and mortality rate assessment
  - C11 BODIPY 581/591 (lipid ROS) analysis in *C. elegans*
  - Mice treatments and toxicity assessment
- QUANTIFICATION AND STATISTICAL ANALYSIS

SUPPLEMENTAL INFORMATION

Supplemental information can be found online at https://doi.org/10.1016/j.chembiol.2023.10.012.

ACKNOWLEDGMENTS

This research was supported by a grant from NCI/NIG to B.R.S. (R35CA209896), as well as by grants from the National Council for Scientific and Technological Development (CNPq-Brazil; grants 405426/2021-6, 303121/2022-0 and INCT-Exposome 406442/2022-3) and Fundação de Amparo à Pesquisa e Inovação do Estado de Santa Catarina (FAPESC Process No: 1367/2022; PJD2022421000102) to M.F. The research was also funded in part through the NIH/NCI Cancer Center Support Grant P30CA013696 and used the Genomics and High Throughput Screening Shared Resource. M.F. thanks the Coordenação de Aperfeiçoamento de Pessoal de Nível Superior-Brazil (CAPES/PRINT-UFSC, Finance Code 001) for a Visiting Research scholarship. J.M. thanks the Fundação de Amparo à Pesquisa e

Inovação do Estado de Santa Catarina (FAPESC Process No: 1367/2022; PJD2022421000102) and CNPq (421702/2022-2; 150727/2023-2) for a post-doctoral scholarship. *C. elegans* strains were provided by the CGC, which is funded by NIH Office of Research Infrastructure Programs (P40 OD010440). Brazilian authors are grateful to the Laboratório Multiusuário de Estudos em Biologia at the Universidade Federal de Santa Catarina (LAMEB/UFSC) for providing its shared infrastructure, as well as to Dr. Luciana A. Honorato and Dr. Thiago M.P. Machado for technical assistance with mice and the voluntary ingestion protocol.

AUTHOR CONTRIBUTIONS

Conceptualization, B.R.S. and M.F.; Methodology, M.F., J.M., A.L.D., A.M.V., E.R., B.R.S., F.Z, R.K.S., M.A.F., N.S., T.H., and M.S. Funding Acquisition, B.R.S. and M.F. Supervision, B.R.S., A.M.V., and M.F. J.M., M.F., and B.R.S. wrote the manuscript with input from all authors.

DECLARATION OF INTERESTS

B.R.S. is an inventor on patents and patent applications involving ferroptosis, holds equity in and serves as a consultant to Exarta Therapeutics, and ProJenX Inc, holds equity in Sonata Therapeutics, and serves as a consultant to Weatherwax Biotechnologies Corporation and Akin Gump Strauss Hauer & Feld LLP.

Received: January 8, 2023
Revised: July 24, 2023
Accepted: October 13, 2023
Published: November 8, 2023

REFERENCES

1. Darshan, D., Frazer, D.M., and Anderson, G.J. (2010). Molecular basis of iron-loading disorders. Expet Rev. Mol. Med. *12*, e36. https://doi.org/10.1017/S1462399410001687.
2. Alexander, J., and Kowdley, K.V. (2009). HFE-associated hereditary hemochromatosis. Genet. Med. *11*, 307–313. https://doi.org/10.1097/GIM.0b013e31819d30f2.
3. Papanikolaou, G., Samuels, M.E., Ludwig, E.H., MacDonald, M.L.E., Franchini, P.L., Dubé, M.P., Andres, L., MacFarlane, J., Sakellaropoulos, N., Politou, M., et al. (2004). Mutations in HFE2 cause iron overload in chromosome 1q–linked juvenile hemochromatosis. Nat. Genet. *36*, 77–82. https://doi.org/10.1038/ng1274.
4. Roetto, A., Totaro, A., Piperno, A., Piga, A., Longo, F., Garozzo, G., Calì, A., De Gobbi, M., Gasparini, P., and Camaschella, C. (2001). New mutations inactivating transferrin receptor 2 in hemochromatosis type 3. Blood *97*, 2555–2560. https://doi.org/10.1182/blood.V97.9.2555.
5. Montosi, G., Donovan, A., Totaro, A., Garuti, C., Pignatti, E., Cassanelli, S., Trenor, C.C., Gasparini, P., Andrews, N.C., and Pietrangelo, A. (2001). Autosomal-dominant hemochrom-atosis is associated with a mutation in the ferroportin (SLC11A3) gene. J. Clin. Invest. *108*, 619–623. https://doi.org/10.1172/JCI200113468.
6. Roetto, A., Papanikolaou, G., Politou, M., Alberti, F., Girelli, D., Christakis, J., Loukopoulos, D., and Camaschella, C. (2003). Mutant antimicrobial peptide hepcidin is associated with severe juvenile hemochromatosis. Nat. Genet. *33*, 21–22. https://doi.org/10.1038/ng1053.
7. Tilney, P.V.R., and Carpenter, H.S. (2014). A 23-Year-Old Woman With a Ferrous Sulfate Overdose. Air Med. J. *33*, 51–54. https://doi.org/10.1016/j.amj.2013.12.006.
8. Halil, H., Tuygun, N., Polat, E., and Karacan, C.D. (2019). Minimum ingested iron cut-off triggering serious iron toxicity in children. Pediatr. Int. *61*, 444–448. https://doi.org/10.1111/ped.13834.
9. Gumber, M.R., Kute, V.B., Shah, P.R., Vanikar, A.V., Patel, H.V., Balwani, M.R., Ghuge, P.P., and Trivedi, H.L. (2013). Successful Treatment of Severe Iron Intoxication with Gastrointestinal Decontamination, Deferoxamine, and Hemodialysis. Ren. Fail. *35*, 729–731. https://doi.org/10.3109/0886022X.2013.790299.
10. Yu, D., and Giffen, M.A. (2021). Suicidal iron overdose: A case report and review of literature. J. Forensic Sci. *66*, 1564–1569. https://doi.org/10.1111/1556-4029.14701.
11. Van Coillie, S., Van San, E., Goetschalckx, I., Wiernicki, B., Mukhopadhyay, B., Tonnus, W., Choi, S.M., Roelandt, R., Dumitrascu, C., Lamberts, L., et al. (2022). Targeting ferroptosis protects against experimental (multi)organ dysfunction and death. Nat. Commun. *13*, 1046. https://doi.org/10.1038/s41467-022-28718-6.
12. Majhail, N.S., Lazarus, H.M., and Burns, L.J. (2008). Iron overload in hematopoietic cell transplantation. Bone Marrow Transplant. *41*, 997–1003. https://doi.org/10.1038/bmt.2008.99.
13. On behalf of the Remacha, Á.F., Remacha, Á.F., Villegas, A., Durán, M.S., Hermosín, L., Hermosín, L., Garcia, M., Diez Campelo, M., and Sanz, G.; IRON-2 Study Group (2015). Evolution of iron overload in patients with low-risk myelodysplastic syndrome: iron chelation therapy and organ complications. Ann. Hematol. *94*, 779–787. https://doi.org/10.1007/s00277-014-2274-y.
14. Zarjou, A., Bolisetty, S., Joseph, R., Traylor, A., Apostolov, E.O., Arosio, P., Balla, J., Verlander, J., Darshan, D., Kuhn, L.C., and Agarwal, A. (2013). Proximal tubule H-ferritin mediates iron trafficking in acute kidney injury. J. Clin. Invest. *123*, 4423–4434. https://doi.org/10.1172/JCI67867.
15. Ward, R.J., Zucca, F.A., Duyn, J.H., Crichton, R.R., and Zecca, L. (2014). The role of iron in brain ageing and neurodegenerative disorders. Lancet Neurol. *13*, 1045–1060. https://doi.org/10.1016/S1474-4422(14)70117-6.
16. Dixon, S.J., Lemberg, K.M., Lamprecht, M.R., Skouta, R., Zaitsev, E.M., Gleason, C.E., Patel, D.N., Bauer, A.J., Cantley, A.M., Yang, W.S., et al. (2012). Ferroptosis: An Iron-Dependent Form of Nonapoptotic Cell Death. Cell *149*, 1060–1072. https://doi.org/10.1016/j.cell.2012.03.042.
17. Jiang, X., Stockwell, B.R., and Conrad, M. (2021). Ferroptosis: mechanisms, biology and role in disease. Nat. Rev. Mol. Cell Biol. *22*, 266–282. https://doi.org/10.1038/s41580-020-00324-8.
18. Friedmann Angeli, J.P., Schneider, M., Proneth, B., Tyurina, Y.Y., Tyurin, V.A., Hammond, V.J., Herbach, N., Aichler, M., Walch, A., Eggenhofer, E., et al. (2014). Inactivation of the ferroptosis regulator Gpx4 triggers acute renal failure in mice. Nat. Cell Biol. *16*, 1180–1191. https://doi.org/10.1038/ncb3064.
19. Tsurusaki, S., Tsuchiya, Y., Koumura, T., Nakasone, M., Sakamoto, T., Matsuoka, M., Imai, H., Yuet-Yin Kok, C., Okochi, H., Nakano, H., et al. (2019). Hepatic ferroptosis plays an important role as the trigger for initiating inflammation in nonalcoholic steatohepatitis. Cell Death Dis. *10*, 449. https://doi.org/10.1038/s41419-019-1678-y.
20. Qi, J., Kim, J.-W., Zhou, Z., Lim, C.-W., and Kim, B. (2020). Ferroptosis Affects the Progression of Nonalcoholic Steatohepatitis via the Modulation of Lipid Peroxidation–Mediated Cell Death in Mice. Am. J. Pathol. *190*, 68–81. https://doi.org/10.1016/j.ajpath.2019.09.011.
21. Shen, D., Wu, W., Liu, J., Lan, T., Xiao, Z., Gai, K., Hu, L., Luo, Z., Wei, C., Wang, X., et al. (2022). Ferroptosis in oligodendrocyte progenitor cells mediates white matter injury after hemorrhagic stroke. Cell Death Dis. *13*, 259. https://doi.org/10.1038/s41419-022-04712-0.
22. Song, L.-M., Xiao, Z.-X., Zhang, N., Yu, X.-Q., Cui, W., Xie, J.-X., and Xu, H.-M. (2021). Apoferritin improves motor deficits in MPTP-treated mice by regulating brain iron metabolism and ferroptosis. iScience *24*, 102431. https://doi.org/10.1016/j.isci.2021.102431.
23. Fisher, S.A., Brunskill, S.J., Doree, C., Chowdhury, O., Gooding, S., and Roberts, D.J. (2013). Oral deferiprone for iron chelation in people with thalassaemia. Cochrane Database Syst. Rev. CD004839. https://doi.org/10.1002/14651858.CD004839.pub3.
24. Bollig, C., Schell, L.K., Rücker, G., Allert, R., Motschall, E., Niemeyer, C.M., Bassler, D., and Meerpohl, J.J. (2017). Deferasirox for managing iron overload in people with thalassaemia. Cochrane Database Syst. Rev. *8*, CD007476. https://doi.org/10.1002/14651858.CD007476.pub3.
25. Adedoyin, O., Boddu, R., Traylor, A., Lever, J.M., Bolisetty, S., George, J.F., and Agarwal, A. (2018). Heme oxygenase-1 mitigates ferroptosis in renal proximal tubule cells. Am. J. Physiol. Ren. Physiol. *314*, F702–F714. https://doi.org/10.1152/ajprenal.00044.2017.

26. Dächert, J., Schoeneberger, H., Rohde, K., and Fulda, S. (2016). RSL3 and Erastin differentially regulate redox signaling to promote Smac mimetic-induced cell death. Oncotarget *7*, 63779–63792. https://doi.org/10.18632/oncotarget.11687.

27. Sun, Y., Zheng, Y., Wang, C., and Liu, Y. (2018). Glutathione depletion induces ferroptosis, autophagy, and premature cell senescence in retinal pigment epithelial cells. Cell Death Dis. *9*, 753. https://doi.org/10.1038/s41419-018-0794-4.

28. Huang, C., and Freter, C. (2015). Lipid Metabolism, Apoptosis and Cancer Therapy. Indian J. Manag. Sci. *16*, 924–949. https://doi.org/10.3390/ijms16010924.

29. Young, R.M., Ackerman, D., Quinn, Z.L., Mancuso, A., Gruber, M., Liu, L., Giannoukos, D.N., Bobrovnikova-Marjon, E., Diehl, J.A., Keith, B., and Simon, M.C. (2013). Dysregulated mTORC1 renders cells critically dependent on desaturated lipids for survival under tumor-like stress. Genes Dev. *27*, 1115–1131. https://doi.org/10.1101/gad.198630.112.

30. Dondelinger, Y., Declercq, W., Montessuit, S., Roelandt, R., Goncalves, A., Bruggeman, I., Hulpiau, P., Weber, K., Sehon, C.A., Marquis, R.W., et al. (2014). MLKL Compromises Plasma Membrane Integrity by Binding to Phosphatidylinositol Phosphates. Cell Rep. *7*, 971–981. https://doi.org/10.1016/j.celrep.2014.04.026.

31. Hildebrand, J.M., Tanzer, M.C., Lucet, I.S., Young, S.N., Spall, S.K., Sharma, P., Pierotti, C., Garnier, J.-M., Dobson, R.C.J., Webb, A.I., et al. (2014). Activation of the pseudokinase MLKL unleashes the four-helix bundle domain to induce membrane localization and necroptotic cell death. Proc. Natl. Acad. Sci. USA *111*, 15072–15077. https://doi.org/10.1073/pnas.1408987111.

32. Magtanong, L., Ko, P.J., and Dixon, S.J. (2016). Emerging roles for lipids in non-apoptotic cell death. Cell Death Differ. *23*, 1099–1109. https://doi.org/10.1038/cdd.2016.25.

33. Nomura, K., Imai, H., Koumura, T., Kobayashi, T., and Nakagawa, Y. (2000). Mitochondrial phospholipid hydroperoxide glutathione peroxidase inhibits the release of cytochrome c from mitochondria by suppressing the peroxidation of cardiolipin in hypoglycaemia-induced apoptosis. Biochem. J. *351*, 183–193. https://doi.org/10.1042/bj3510183.

34. Garrido, C., Galluzzi, L., Brunet, M., Puig, P.E., Didelot, C., and Kroemer, G. (2006). Mechanisms of cytochrome c release from mitochondria. Cell Death Differ. *13*, 1423–1433. https://doi.org/10.1038/sj.cdd.4401950.

35. Epand, R.F., Martinou, J.-C., Montessuit, S., and Epand, R.M. (2004). Fatty acids enhance membrane permeabilization by pro-apoptotic Bax. Biochem. J. *377*, 509–516. https://doi.org/10.1042/bj20030938.

36. Dixon, S.J., Winter, G.E., Musavi, L.S., Lee, E.D., Snijder, B., Rebsamen, M., Superti-Furga, G., and Stockwell, B.R. (2015). Human Haploid Cell Genetics Reveals Roles for Lipid Metabolism Genes in Nonapoptotic Cell Death. ACS Chem. Biol. *10*, 1604–1609. https://doi.org/10.1021/acschembio.5b00245.

37. Yuan, H., Li, X., Zhang, X., Kang, R., and Tang, D. (2016). Identification of ACSL4 as a biomarker and contributor of ferroptosis. Biochem. Biophys. Res. Commun. *478*, 1338–1343. https://doi.org/10.1016/j.bbrc.2016.08.124.

38. Kagan, V.E., Mao, G., Qu, F., Angeli, J.P.F., Doll, S., Croix, C.S., Dar, H.H., Liu, B., Tyurin, V.A., Ritov, V.B., et al. (2017). Oxidized arachidonic and adrenic PEs navigate cells to ferroptosis. Nat. Chem. Biol. *13*, 81–90. https://doi.org/10.1038/nchembio.2238.

39. Venkatesh, D., O'Brien, N.A., Zandkarimi, F., Tong, D.R., Stokes, M.E., Dunn, D.E., Kengmana, E.S., Aron, A.T., Klein, A.M., Csuka, J.M., et al. (2020). MDM2 and MDMX promote ferroptosis by PPARα-mediated lipid remodeling. Genes Dev. *34*, 526–543. https://doi.org/10.1101/gad.334219.119.

40. Tao, P., Jiang, Y., Wang, H., and Gao, G. (2021). CYP2J2-produced epoxyeicosatrienoic acids contribute to the ferroptosis resistance of pancreatic ductal adenocarcinoma in a PPARγ-dependent manner. Zhong Nan Da Xue Xue Bao Yi Xue Ban *46*, 932–941. https://doi.org/10.11817/j.issn.1672-7347.2021.210413.

41. Xing, G., Meng, L., Cao, S., Liu, S., Wu, J., Li, Q., Huang, W., and Zhang, L. (2022). PPARα alleviates iron overload-induced ferroptosis in mouse liver. EMBO Rep. *23*, e52280. https://doi.org/10.15252/embr.202052280.

42. Magtanong, L., Ko, P.-J., To, M., Cao, J.Y., Forcina, G.C., Tarangelo, A., Ward, C.C., Cho, K., Patti, G.J., Nomura, D.K., et al. (2019). Exogenous Monounsaturated Fatty Acids Promote a Ferroptosis-Resistant Cell State. Cell Chem. Biol. *26*, 420–432.e9. https://doi.org/10.1016/j.chembiol.2018.11.016.

43. Lin, Z., Liu, J., Long, F., Kang, R., Kroemer, G., Tang, D., and Yang, M. (2022). The lipid flippase SLC47A1 blocks metabolic vulnerability to ferroptosis. Nat. Commun. *13*, 7965. https://doi.org/10.1038/s41467-022-35707-2.

44. Skouta, R., Dixon, S.J., Wang, J., Dunn, D.E., Orman, M., Shimada, K., Rosenberg, P.A., Lo, D.C., Weinberg, J.M., Linkermann, A., and Stockwell, B.R. (2014). Ferrostatins Inhibit Oxidative Lipid Damage and Cell Death in Diverse Disease Models. J. Am. Chem. Soc. *136*, 4551–4556. https://doi.org/10.1021/ja411006a.

45. Hassannia, B., Wiernicki, B., Ingold, I., Qu, F., Van Herck, S., Tyurina, Y.Y., Bayır, H., Abhari, B.A., Angeli, J.P.F., Choi, S.M., et al. (2018). Nano-targeted induction of dual ferroptotic mechanisms eradicates high-risk neuroblastoma. J. Clin. Invest. *128*, 3341–3355. https://doi.org/10.1172/JCI99032.

46. Dimov, I., and Maduro, M.F. (2019). The C. elegans intestine: organogenesis, digestion, and physiology. Cell Tissue Res. *377*, 383–396. https://doi.org/10.1007/s00441-019-03036-4.

47. Stockwell, B.R., Friedmann Angeli, J.P., Bayir, H., Bush, A.I., Conrad, M., Dixon, S.J., Fulda, S., Gascón, S., Hatzios, S.K., Kagan, V.E., et al. (2017). Ferroptosis: A Regulated Cell Death Nexus Linking Metabolism, Redox Biology, and Disease. Cell *171*, 273–285. https://doi.org/10.1016/j.cell.2017.09.021.

48. Yang, W.S., Kim, K.J., Gaschler, M.M., Patel, M., Shchepinov, M.S., and Stockwell, B.R. (2016). Peroxidation of polyunsaturated fatty acids by lipoxygenases drives ferroptosis. Proc. Natl. Acad. Sci. USA *113*, E4966–E4975. https://doi.org/10.1073/pnas.1603244113.

49. Perez, M.A., Magtanong, L., Dixon, S.J., and Watts, J.L. (2020). Dietary Lipids Induce Ferroptosis in Caenorhabditiselegans and Human Cancer Cells. Dev. Cell *54*, 447–454.e4. https://doi.org/10.1016/j.devcel.2020.06.019.

50. Qin, S., Wang, Y., Li, L., Liu, J., Xiao, C., Duan, D., Hao, W., Qin, C., Chen, J., Yao, L., et al. (2022). Early-life vitamin B12 orchestrates lipid peroxidation to ensure reproductive success via SBP-1/SREBP1 in Caenorhabditis elegans. Cell Rep. *40*, 111381. https://doi.org/10.1016/j.celrep.2022.111381.

51. Sunshine, H., and Iruela-Arispe, M.L. (2017). Membrane lipids and cell signaling. Curr. Opin. Lipidol. *28*, 408–413. https://doi.org/10.1097/MOL.0000000000000443.

52. Alvaro, A., Rosales, R., Masana, L., and Vallvé, J.C. (2010). Polyunsaturated fatty acids down-regulate *in vitro* expression of the key intestinal cholesterol absorption protein NPC1L1: no effect of monounsaturated nor saturated fatty acids. J. Nutr. Biochem. *21*, 518–525. https://doi.org/10.1016/j.jnutbio.2009.02.010.

53. Georgiadi, A., and Kersten, S. (2012). Mechanisms of Gene Regulation by Fatty Acids. Adv. Nutr. *3*, 127–134. https://doi.org/10.3945/an.111.001602.

54. Ingold, I., Berndt, C., Schmitt, S., Doll, S., Poschmann, G., Buday, K., Roveri, A., Peng, X., Porto Freitas, F., Seibt, T., et al. (2018). Selenium Utilization by GPX4 Is Required to Prevent Hydroperoxide-Induced Ferroptosis. Cell *172*, 409–422.e21. https://doi.org/10.1016/j.cell.2017.11.048.

55. Magtanong, L., Mueller, G.D., Williams, K.J., Billmann, M., Chan, K., Armenta, D.A., Pope, L.E., Moffat, J., Boone, C., Myers, C.L., et al. (2022). Context-dependent regulation of ferroptosis sensitivity. Cell Chem. Biol. *29*, 1409–1418.e6. https://doi.org/10.1016/j.chembiol.2022.06.004.

56. Bersuker, K., Hendricks, J.M., Li, Z., Magtanong, L., Ford, B., Tang, P.H., Roberts, M.A., Tong, B., Maimone, T.J., Zoncu, R., et al. (2019). The CoQ

oxidoreductase FSP1 acts parallel to GPX4 to inhibit ferroptosis. Nature *575*, 688–692. https://doi.org/10.1038/s41586-019-1705-2.

57. Wu, J., Shao, X., Shen, J., Lin, Q., Zhu, X., Li, S., Li, J., Zhou, W., Qi, C., and Ni, Z. (2022). Downregulation of PPARα mediates FABP1 expression, contributing to IgA nephropathy by stimulating ferroptosis in human mesangial cells. Int. J. Biol. Sci. *18*, 5438–5458. https://doi.org/10.7150/ijbs.74675.
58. Cao, A., Li, H., Zhou, Y., Wu, M., and Liu, J. (2010). Long Chain Acyl-CoA Synthetase-3 Is a Molecular Target for Peroxisome Proliferator-activated Receptor δ in HepG2 Hepatoma Cells. J. Biol. Chem. *285*, 16664–16674. https://doi.org/10.1074/jbc.M110.112805.
59. Van Gilst, M.R., Hadjivassiliou, H., Jolly, A., and Yamamoto, K.R. (2005). Nuclear Hormone Receptor NHR-49 Controls Fat Consumption and Fatty Acid Composition in C. elegans. PLoS Biol. *3*, e53. https://doi.org/10.1371/journal.pbio.0030053.
60. Atherton, H.J., Jones, O.A.H., Malik, S., Miska, E.A., and Griffin, J.L. (2008). A comparative metabolomic study of NHR-49 in *Caenorhabditis elegans* and PPAR-α in the mouse. FEBS Lett. *582*, 1661–1666. https://doi.org/10.1016/j.febslet.2008.04.020.
61. Webster, C.M., Deline, M.L., and Watts, J.L. (2013). Stress response pathways protect germ cells from omega-6 polyunsaturated fatty acid-mediated toxicity in Caenorhabditis elegans. Dev. Biol. *373*, 14–25. https://doi.org/10.1016/j.ydbio.2012.10.002.
62. Braughler, J.M., Duncan, L.A., and Chase, R.L. (1986). The involvement of iron in lipid peroxidation. Importance of ferric to ferrous ratios in initiation. J. Biol. Chem. *261*, 10282–10289. https://doi.org/10.1016/S0021-9258(18)67521-0.
63. Stockwell, B.R., and Jiang, X. (2020). The Chemistry and Biology of Ferroptosis. Cell Chem. Biol. *27*, 365–375. https://doi.org/10.1016/j.chembiol.2020.03.013.
64. Jenkins, N.L., James, S.A., Salim, A., Sumardy, F., Speed, T.P., Conrad, M., Richardson, D.R., Bush, A.I., and McColl, G. (2020). Changes in ferrous iron and glutathione promote ferroptosis and frailty in aging Caenorhabditis elegans. Elife *9*, e56580. https://doi.org/10.7554/eLife.56580.
65. Perez, M.A., Clostio, A.J., Houston, I.R., Ruiz, J., Magtanong, L., Dixon, S.J., and Watts, J.L. (2022). Ether lipid deficiency disrupts lipid homeostasis leading to ferroptosis sensitivity. PLoS Genet. *18*, e1010436. https://doi.org/10.1371/journal.pgen.1010436.
66. Sarparast, M., Pourmand, E., Hinman, J., Vonarx, D., Reason, T., Zhang, F., Paithankar, S., Chen, B., Borhan, B., Watts, J.L., et al. (2023). Dihydroxy-Metabolites of Dihomo-gamma-linolenic Acid Drive Ferroptosis-Mediated Neurodegeneration. Preprint at bioRxiv. https://doi.org/10.1101/2023.01.05.522933.
67. Cui, W., Liu, D., Gu, W., and Chu, B. (2021). Peroxisome-driven ether-linked phospholipids biosynthesis is essential for ferroptosis. Cell Death Differ. *28*, 2536–2551. https://doi.org/10.1038/s41418-021-00769-0.
68. Zou, Y., Henry, W.S., Ricq, E.L., Graham, E.T., Phadnis, V.V., Maretich, P., Paradkar, S., Boehnke, N., Deik, A.A., Reinhardt, F., et al. (2020). Plasticity of ether lipids promotes ferroptosis susceptibility and evasion. Nature *585*, 603–608. https://doi.org/10.1038/s41586-020-2732-8.
69. Brenner, S. (1974). THE GENETICS OF *CAENORHABDITIS ELEGANS*. Genetics *77*, 71–94. https://doi.org/10.1093/genetics/77.1.71.
70. Porta-de-la-Riva, M., Fontrodona, L., Villanueva, A., and Cerón, J. (2012). Basic Caenorhabditis elegans Methods: Synchronization and Observation. JoVE *64*, 4019. https://doi.org/10.3791/4019.
71. Percie du Sert, N., Alfieri, A., Allan, S.M., Carswell, H.V., Deuchar, G.A., Farr, T.D., Flecknell, P., Gallagher, L., Gibson, C.L., Haley, M.J., et al. (2017). The IMPROVE Guidelines (Ischaemia Models: Procedural Refinements Of in Vivo Experiments). J. Cerebr. Blood Flow Metabol. *37*, 3488–3517. https://doi.org/10.1177/0271678X17709185.
72. Bray, N., Pimentel, H., Melsted, P., and Pachter, L. (2016). Near-optimal probabilistic RNA-seq quantification. Nat Biotechnol *34*, 525–527.
73. Pimentel, H., Bray, N.L., Puente, S., Melsted, P., and Pachter, L. (2017). Differential analysis of RNA-seq incorporating quantification uncertainty. Nat. Methods *14*, 687–690. https://doi.org/10.1038/nmeth.4324.
74. Meier, F., Brunner, A.-D., Frank, M., Ha, A., Bludau, I., Voytik, E., Kaspar-Schoenefeld, S., Lubeck, M., Raether, O., Bache, N., et al. (2020). diaPASEF: parallel accumulation–serial fragmentation combined with data-independent acquisition. Nat. Methods *17*, 1229–1236. https://doi.org/10.1038/s41592-020-00998-0.
75. Kulak, N.A., Pichler, G., Paron, I., Nagaraj, N., and Mann, M. (2014). Minimal, encapsulated proteomic-sample processing applied to copy-number estimation in eukaryotic cells. Nat. Methods *11*, 319–324. https://doi.org/10.1038/nmeth.2834.
76. Demichev, V., Messner, C.B., Vernardis, S.I., Lilley, K.S., and Ralser, M. (2020). DIA-NN: neural networks and interference correction enable deep proteome coverage in high throughput. Nat. Methods *17*, 41–44. https://doi.org/10.1038/s41592-019-0638-x.
77. Lakowski, B., and Hekimi, S. (1998). The genetics of caloric restriction in *Caenorhabditis elegans*. Proc. Natl. Acad. Sci. USA *95*, 13091–13096. https://doi.org/10.1073/pnas.95.22.13091.
78. Deline, M.L., Vrablik, T.L., and Watts, J.L. (2013). Dietary Supplementation of Polyunsaturated Fatty Acids in Caenorhabditis elegans. JoVE, 50879. https://doi.org/10.3791/50879.
79. Beaudoin-Chabot, C., Wang, L., Smarun, A.V., Vidović, D., Shchepinov, M.S., and Thibault, G. (2019). Deuterated Polyunsaturated Fatty Acids Reduce Oxidative Stress and Extend the Lifespan of C. elegans. Front. Physiol. *10*, 641. https://doi.org/10.3389/fphys.2019.00641.
80. Bolsoni-Lopes, A., Festuccia, W.T., Chimin, P., Farias, T.S.M., Torres-Leal, F.L., Cruz, M.M., Andrade, P.B., Hirabara, S.M., Lima, F.B., and Alonso-Vale, M.I.C. (2014). Palmitoleic acid (n-7) increases white adipocytes GLUT4 content and glucose uptake in association with AMPK activation. Lipids Health Dis. *13*, 199. https://doi.org/10.1186/1476-511X-13-199.
81. Scarborough, J., Mueller, F., Arban, R., Dorner-Ciossek, C., Weber-Stadlbauer, U., Rosenbrock, H., Meyer, U., and Richetto, J. (2020). Preclinical validation of the micropipette-guided drug administration (MDA) method in the maternal immune activation model of neurodevelopmental disorders. Brain Behav. Immun. *88*, 461–470. https://doi.org/10.1016/j.bbi.2020.04.015.
82. Franco, J.L., Posser, T., Dunkley, P.R., Dickson, P.W., Mattos, J.J., Martins, R., Bainy, A.C.D., Marques, M.R., Dafre, A.L., and Farina, M. (2009). Methylmercury neurotoxicity is associated with inhibition of the antioxidant enzyme glutathione peroxidase. Free Radic. Biol. Med. *47*, 449–457. https://doi.org/10.1016/j.freeradbiomed.2009.05.013.

Please cite this article in press as: Mann et al., Ferroptosis inhibition by oleic acid mitigates iron-overload-induced injury, Cell Chemical Biology (2023), https://doi.org/10.1016/j.chembiol.2023.10.012

STAR★METHODS

KEY RESOURCES TABLE

REAGENT or RESOURCE	SOURCE	IDENTIFIER
Antibodies		
Mouse monoclonal anti-ACSL4 antibody	Santa Cruz Biotechnology	Cat# sc-365230; RRID:AB_10843105
Mouse monoclonal anti-alpha-tubulin antibody	Santa Cruz Biotechnology	Cat# sc-32293; RRID:AB_628412
Mouse monoclonal anti-Glutathione Peroxidase 4 antibody	R&D Systems	Cat# MAB5457; RRID:AB_2232542
Rabbit polyclonal anti-AIFM2/FSP1 antibody	Proteintech	Cat# 20886-1-AP; RRID:AB_2878756
Rabbit polyclonal anti-GAPDH antibody	Abcam	Cat# ab9485; RRID: AB_307275
Rabbit polyclonal anti-xCT antibody	Abcam	Cat# ab37185; RRID:AB_778944
Rabbit monoclonal anti-SLC47A1 antibody	Cell Signaling	Cat# 14550S
Rabbit polyclonal anti-ACSL3 antibody	Abcam	Cat# ab151959
IRDye® 680LT Goat anti-Mouse IgG Secondary Antibody	LI-COR	Cat# 926-68020; RRID AB_2651127
IRDye® 800CW Goat anti-Rabbit IgG Secondary Antibody	LI-COR	Cat# 925-32211; RRID AB_10706161
Bacterial and virus strains		
Escherichia coli - OP50	Caenorhabditis Genetics Center	OP50
Chemicals, peptides, and recombinant proteins		
ABT-199	Cayman Chemical	Cat# 16233; CAS: 1257044-40-8
Ammonium iron(III) citrate	Sigma-Aldrich	Cat# F5879; CAS: 1185-57-5
Antibiotic Antimycotic Solution (100×), Stabilized	Sigma-Aldrich	Cat# A5955
Arachidonic acid (cell treatment)	Cayman Chemical	Cat# 90010; CAS: 506-32-1
BODIPY™ 581/591 undecanoic acid	Invitrogen	Cat# D3861
CellTiter-Glo® Luminescent Cell Viability Assay	Promega	Cat# G7570
Dimethyl sulfoxide	Sigma-Aldrich	Cat# 276855; CAS: 67-68-5
DL-Dithiothreitol	Sigma-Aldrich	Cat# D0632; CAS 3483-12-3
Dulbecco's Modified Eagle's/Ham's F-12 Medium 1:1 (DMEF)	Caisson Labs	Cat# DFL13-500ML
Eagle's Minimum Essential Medium (EMEM)	Gibco	Cat# 11095072
Ferrostatin-1	Sigma-Aldrich	Cat# SML0583; CAS: 347174-05-4
GW6471	Sigma-Aldrich	Cat# G5045; CAS: 880635-03-0
LCL-161	Cayman Chemical	Cat# 22420; CAS: 1005342-46-0
Linoleic acid (cell treatment)	Cayman Chemical	Cat# 90150; CAS: 60-33-3
Linoleic acid (worm treatment)	Sigma-Aldrich	Cat# W800075; CAS: 60-33-3
Necrostatin-1s (Necrostatin 2 racemate)	Selleck Chemicals	Cat# S8641; CAS: 852391-15-2
Necrosulfonamide	Selleck Chemicals	Cat# S8251; CAS: 1360614-48-7
Oleic acid (cell treatment)	Cayman Chemical	Cat# Cat# 90260; CAS: 112-80-1
Oleic acid (worms and mice treatment)	Labsynth	Cat# 01A1048.01.BJ
Recombinant Human TNF-α	Peprotech	Cat# 300-01A

(*Continued on next page*)

Please cite this article in press as: Mann et al., Ferroptosis inhibition by oleic acid mitigates iron-overload-induced injury, Cell Chemical Biology (2023), https://doi.org/10.1016/j.chembiol.2023.10.012

Continued

REAGENT or RESOURCE	SOURCE	IDENTIFIER
RSL3 (1S,3R-RSL 3)	Sigma-Aldrich	Cat# SML2234; CAS: 1219810-16-8
Stearic acid (cell treatment)	Cayman Chemical	Cat# 10011298; CAS: 57-11-4
Stearic acid (worm treatment)	Labsynth	Cat# 00A1030.06.AG
T0070907	Sigma-Aldrich	Cat# T8703; CAS: 313516-66-4
Tergitol	Sigma-Aldrich	Cat# NP40S
2-Thiobarbituric acid	Sigma-Aldrich	T5500
Z-VAD-FMK	Selleck Chemicals	Cat# S7023; CAS: 187389-52-2
Critical commercial assays		
LDH - lactate dehydrogenase kit	Labtest Diagnóstica S.A.	Ref. 86
ALT - aspartate aminotransferase kit	Labtest Diagnóstica S.A.	Ref. 108
Deposited data		
Bulk RNAseq	GEO	GSE243891
Proteomics	ProteomeXchange	PXD045642
Lipidomics	MetaboLights	MTBLS8664
Experimental models: Cell lines		
HEK-293	ATCC	CRL-1573
Hep G2	ATCC	HB-8065
SK-N-Be(2)	ATCC	CRL-2271
Experimental models: Organisms/strains		
C. elegans: Strain N2 Bristol (wild-type)	Caenorhabditis Genetics Center	Cat# N2
C. elegans: Strain STE68 nhr-49(nr2041) I	Caenorhabditis Genetics Center	Cat# STE68
Mouse (*Mus musculus*): Strain *Swiss*	Federal University of Santa Catarina, Brazil	N/A
Software and algorithms		
FlowJo 10.1r5	Becton, Dickinson & Company	https://www.flowjo.com/
ImageJ 1.48v	Rasband, W.S.	https://imagej.nih.gov/ij/
Prism 9.0	GraphPad Software	https://www.graphpad.com/features
Progenesis QI software	Waters Corporation	https://www.nonlinear.com/progenesis/qi/
MSe Viewer	Waters Corporation	https://www.waters.com/waters/educationInstance.htm?eiid=134791102
Metaboanalyst (v 5.0)	–	https://www.metaboanalyst.ca/

RESOURCE AVAILABILITY

Lead contact

Further information and requests for resources and reagents should be directed to and will be fulfilled by the Lead Contact, Brent R. Stockwell (bstockwell@columbia.edu).

Materials availability

Antibodies, reagents and cell lines used for biological studies were obtained from commercial or internal sources described in the key resources table. Where available these may be shared by the lead contact. This study did not generate new unique reagents.

Data and code availability

- Bulk RNAseq data have been deposited at GEO, accession numbers listed in the key resources table. Proteomics data have been deposited to PRIDE and are available via ProteomeXchange Consortium with identifier listed in the key resources table. Metabolomics is being deposited to MetaboLights, study number listed in key resources table. All data reported in this paper will be shared by the lead contact upon request.
- This paper does not report any original code.
- Any additional information required to reanalyze the data reported in this paper is available from the lead contact upon request.

Please cite this article in press as: Mann et al., Ferroptosis inhibition by oleic acid mitigates iron-overload-induced injury, Cell Chemical Biology (2023), https://doi.org/10.1016/j.chembiol.2023.10.012

EXPERIMENTAL MODEL AND STUDY PARTICIPANT DETAILS

Cell lines and culture conditions

HEK-293, Hep G2 and SK-N-Be(2) cells were purchased from ATCC, expanded for one passage and frozen at approximately -140°C for use in subsequent experiments. HEK-293 and Hep G2 cells were grown in Minimum Essential Medium (MEM, Cat # 11095072, Gibco) supplemented with 10% fetal bovine serum (FBS, Cat# 26140-079, Gibco) and antibiotic-antimycotic (100 units penicillin, 0.1 mg streptomycin and 2.5 ng amphotericin B per mL, Cat# A5955, Sigma-Aldrich). SK-N-Be(2) cells were grown in Dulbecco's Modified Eagle's/Ham's F-12 Medium 1:1 (DMEF, cat# DFL13-500ML, Caisson Labs) supplemented with 10% FBS and antibiotic-antimycotic. Cells were maintained at 37°C in a humidified atmosphere containing 5% CO_2. For all experiments, cells were trypsinized (0.25% Trypsin-EDTA solution, Cat# 25200114, Gibco) and counted using a Vi-CELL XR cell counter (Beckman Coulter, Inc., Fullerton, CA).

C. elegans strains and conditions

Worms were cultivated for 2–3 generations without starvation at 20°C in plates containing nematode growth media (NGM) agar seeded with *Escherichia coli* strain OP50.[69] The N2 and STE68 nhr-49(nr2041) I strains were purchased from the *Caenorhaditis* Genetics Center (CGC). All experiments were performed using hermaphrodites. Synchronization of nematode cultures was achieved via hypochlorite bleaching of gravid hermaphrodites using standard protocol.[70]

Mice

Animals were monitored in accordance with the IMPROVE guidelines[71] and the experimental protocol was approved by the Animal Use Ethics Committee of the Federal University of Santa Catarina (UFSC, Florianopolis, Brazil) - protocol number 3550051019 (ID 001488). Adult male Swiss mice (70 days old; n = 28), weighing approximately 45 g, were obtained from the animal facility of UFSC. Only male mice were used and the influence of sex was not evaluated considering the previous standardization of this *in vivo* model. Animals were kept in standard polypropylene cages (40 x 32 x 17 cm) with freely available water and food (Nuvilab CR-1 - Quimtia) within a 12 h light/dark cycle (6 a.m./6 p.m.).

METHOD DETAILS

Cell viability assessment

HEK-293, Hep G2 and SK-N-Be(2) cells were plated at 2,000 cells per well in white 384-well plates (Cat# 6007619 PerkinElmer) (40 μL per well) in triplicate and incubated for 24h. The cells were then treated with different concentrations of ferric ammonium citrate (FAC), as well as classic ferroptosis (50 nM RSL3) and apoptosis (100 μM ABT-199) inducers. Necroptosis was induced by treatment with 100 μM Z-VAD-FMK, followed by 30 minutes of incubation and additional treatment with 50 ng/mL TNF-α plus 100 μM LCL-161. Co-treatments with classic anti-ferroptotic (5 μM ferrostatin-1), anti-apoptotic (100 μM Z-VAD-FMK) or anti-necroptotic (50 μM necrostatin-1s + 1 μM necrosulfonamide) agents were also performed. Compounds were dissolved in culture medium containing DMSO, whose maximum final concentration was 0.3%. Treatment volume was 10 μL, culminating in a final volume of 50 μL per well (40 μL of cell medium + 10 μL of treatments). At different time-points, cell viability was assessed by adding 40 μL of 50% CellTiter-Glo (Promega) 50% cell culture medium to each well. After incubation at room temperature with shaking for 10 min, luminescence was measured using a Victor X5 plate reader (PerkinElmer). All cell viability data were normalized to the DMSO vehicle condition.

For fatty acids (FAs)-exposed cells, treatments with stearic, oleic, linoleic, or arachidonic acids (0-400 μM) were performed at 90 minutes after seeding. Fatty acids were dissolved in cell culture medium containing ethanol, whose final concentration was 0.5%. Control cells received just vehicle (ethanol). 24 h after seeding, FAC treatment was performed as described above.

To investigate the relationship between the effects of GW6471 and oleic acid, HEK-293 cells were plated at 10,000 cells per well in white 96-well plates (Cat# 136101 Thermo Fisher) at final volume of 200 μL per well in quadruplicate. Oleic acid (12.5 μM) was added to half of the wells after 90 minutes, and all plates were incubated for 24h at 37°C and 5% CO_2. Cells were then treated with either vehicle (DMSO, 0.5% max), RSL3 (0.1 μM), GW6471 (10 μM), or both RSL3 and GW6471 for 24 hours, and cell viability was assessed by adding 50 μL of 1:1 mixture CellTiter-Glo (Promega):cell culture medium to each well. After incubation at room temperature with shaking for 10 min, luminescence was measured using a Victor X5 plate reader (PerkinElmer).

Lipid ROS assay using flow cytometer

For flow cytometry experiments, cells were seeded at a density of 350,000 cells/well in 6 well-plates (Cat# 3335, Corning). In experiments investigating the role of oleic acid, cells were treated with vehicle (ethanol) or 50 μM oleic acid at 90 minutes after seeding. 24 h after seeding, cells were treated with FAC (16 mM) and/or Fer-1 (5 μM). After 6 h, cells were harvested by trypsinization (500 μL) and transferred to a 5-mL microfuge tube containing 2 mL of culture medium supplemented with 10% SFB. Cells were then pelleted (250 x *g*, 5 min) and resuspended in C11 BODIPY 581/591 (2 μM) dissolved in HBSS. Cell suspensions were incubated at 37 C for 10 min. Thereafter, the cells were pelleted (250 x *g*, 5 min) and resuspended in 100 μL HBSS. Using a Beckman CytoFLEX System B4-R0-V0 flow cytometer, fluorescence intensity was measured on the FL1 channel with gating to record live cells only (gate constructed from control group). A minimum of 10,000 cells were analyzed per condition. Analysis was performed using FlowJo software.

Please cite this article in press as: Mann et al., Ferroptosis inhibition by oleic acid mitigates iron-overload-induced injury, Cell Chemical Biology (2023), https://doi.org/10.1016/j.chembiol.2023.10.012

Western blot analysis

HEK-293, Hep G2 and SK-N-Be(2) cells were seeded at a density of 350,000 cells/well in 6 well-plates (Cat# 3335, Corning). After 90 min, cells were treated with vehicle (ethanol) or 50 μM oleic acid. Twenty-four h after seeding, cells were treated with 16 mM FAC. After 4 h, the media was removed and cells were washed once with 2 mL PBS. After washing, cells were scraped off the plate in 100 μL of RIPA lysis/extraction buffer (Cat# 89900, ThermoFisher Scientific) containing protease inhibitor cocktail (Cat# 11836153001, Roche). After 30 minutes of agitation on ice, lysates were sonicated and spun down to remove any debris (10,000 x *g*, 10 min, room temperature or 4°C). Clarified lysates were transferred to a new 1.5 mL tube. Protein concentration in lysates was quantified using Bradford's assay (Bradford Protein Assay Dye Reagent Concentrate, Cat# 5000006, Bio-Rad, Hercules, CA) with a standard bovine serum albumin curve. Equal amounts of protein were combined with 4x Laemmli Sample Buffer (Cat# 1610747, Bio-Rad) and 50 mM dithiothreitol (Cat# D0632, Sigma-Aldrich). Protein was denatured by boiling for 5 min and loaded onto a Bolt 4-12% Bis-Tris Plus Gel (Cat# NW04122BOX) (Life Technologies). Protein was transferred to a nitrocellulose membrane using an iBlot2 transfer stack (Life Technologies). The membrane was blocked using Intercept® (PBS) Blocking Buffer (Cat# 927-70001, LI-COR Biotechnology) (1 h, room temperature) and then incubated in primary antibody mixture (18 h, 4°C). Primary antibodies used were anti-ACSL4 (Cat# sc-365230, Santa Cruz Biotechnology; 1:1000 dilution), anti-alpha-tubulin (Cat# sc-32293, Santa Cruz Biotechnology; 1:5000 dilution), anti-GPX4 (Cat# MAB5457, R&D Systems; 1:500 dilution), anti-AIFM2/FSP1 (Cat# 20886-1-AP, Proteintech; 1:500 dilution), anti-GAPDH (Cat# ab9485, Abcam; 1: 5000 dilution), anti-xCT (Cat# ab37185, Abcam; 1:350 dilution). The membrane was washed 3x in TBST and incubated with secondary antibodies (1 h, room temperature). Secondary antibodies used were goat anti-rabbit (Cat# 925-32211, LI-COR Biotechnology, 1:4000 dilution) and goat anti-mouse (Cat# 926-68020, LI-COR, 1:15000 dilution), and the secondary antibody buffer was 1:1 Blocking Buffer:TBST solution. The membrane was washed 3 times in TBST and scanned on a LICOR Odyssey 9120 Imaging System with image acquisition and export using Image Studio (ver. 3.0). In order to investigate the effects of GW6471 in ACSL3 and SLC47A1 protein levels, $1x10^6$ HEK-293 cells were seeded in 10 cM dishes; appropriate plates were treated with oleic acid (12.5 or 25 μM) 90 minutes later, and all plates were subsequently incubated for 24h at 37°C and 5% CO_2. Cells were then treated with either DMSO (0.3% max) or GW6471 (15 μM) for 24 hours. Subsequent western blotting procedure identical to the previous mentioned conditions. Primary antibodies used were anti-SLC47A1 (Cell Signaling, #14550S), anti-ACSL3 (Cat # ab151959, Abcam, 1:250 dilution) and anti-β-actin (Cat #3700T, Cell Signaling, 1:250 dilution).

Lipidomic analyses

HEK-293 cells (four independent biological replicates per treatment) were seeded in 100 mm culture dishes at a density of $5x10^6$ per dish (Cat# 430167, Corning). After 90 min, cells were treated with vehicle (ethanol) or 50 μM oleic acid. Twenty-four h after seeding, cells were treated with 16 mM FAC. After 4 h, the media was removed and cells were washed twice with ice-cold PBS (2 mL) to remove the media while keeping the plate on ice. Cells were then scraped in 3 mL of ice-cold PBS containing butylated hydroxyl toluene (BHT, 0.001% w/v in ethanol) and transferred to pre-cold 5-mL tubes. After vortexing, a 300 μL aliquot was taken for protein analysis and the remaining volume (approximately 1.7 mL) was centrifuged at 350 x *g* for 5 min at 4°C. After centrifugation, the supernatant was aspirated and the pellet was stored at -80°C. In the next day, samples were mixed with 1 μl of SPLASH lipidomics internal standard mix (Avanti Polar Lipids, Inc.) with a microtip solicitor. After homogenization, samples were transferred to glass vials containing 850 μl of cold methyl-tert-butyl ether (MTBE) and vortex-mixed for 30 s. A 2 h incubation (on ice) was performed to improve the lipid extraction efficiency. Thereafter, 200 μl of ice-cold water were added and the samples were incubated on ice for 20 min. After centrifugation (3,000 r.p.m. for 20 min at 4°C), the lipid-containing upper phase was collected and dried down under a gentle stream of nitrogen gas. A mixture of 2-propanol/acetonitrile/water (4:3:1, v/v/v and 0.01% butylated hydroxytoluene) was used to reconstitute the dried samples before liquid chromatography–mass spectrometry (LC–MS) analysis. A quality control sample was prepared by combining 40 μl of each sample to assess the reproducibility of the features through the runs.

LC conditions

Lipids were separated using an Acquity UPLC CSH column (2.1 × 100 mm, 1.7 μm) over a 20-min gradient elution on a Waters Acquity UPLC I-Class system. Mobile phases A [acetonitrile/water (60:40, v/v)] and B [2-propanol/acetonitrile/water (85:10:5, v/v/v)] contained 0.1% acetic acid and 10 mM ammonium acetate. Following the injections, the gradient was held at 40% mobile phase B for 2 min. At 2.1 min, it reached to 50% B, then increased to 70% B in 12 min, at 12.1 min changed to 70% B and at 18 min increased to 90% B. The eluent composition returned to the initial condition in 1 min, and the column was re-equilibrated for an additional 1 min before the next injection was conducted. The oven temperature was set at 55°C and the flow rate was 400 μl min^{-1}. The flow-through needle mode was used to allow for injections of 6 μl. The quality control sample was injected between the samples and at the beginning and end of the run to monitor the performance and the stability of the MS platform.

MS conditions

The SYNAPT G2-Si -Q-ToF mass spectrometer was operated in both positive and negative electrospray ionization modes. For the positive mode, a capillary voltage and sampling cone voltage of 2 kV and 32 V were used. The source and desolvation temperatures were kept at 120 and 500°C, respectively. Nitrogen was used as the desolvation gas with a flow rate of 800 l h^{-1}. For the negative mode, a capillary voltage of 1.5 kV and a cone voltage of 30 V were used. The source temperature was 120°C and the desolvation gas flow was set to 800 l h^{-1}. Depending on the ionization mode, the protonated molecular ion of leucine encephalin ($[M + H]^+$, mass to

Please cite this article in press as: Mann et al., Ferroptosis inhibition by oleic acid mitigates iron-overload-induced injury, Cell Chemical Biology (2023), https://doi.org/10.1016/j.chembiol.2023.10.012

charge ratio (*m/z*): 556.2771) or the deprotonated molecular ion ($[M - H]^-$, *m/z*: 554.2615) was used as a lock mass for mass accuracy and reproducibility. The data were collected in duplicates in data-independent (MS^E) mode over the mass range *m/z*: 50 to 1,200 Da. The quality control sample was also acquired in enhanced data-independent ion mobility (HDMSE) in both positive and negative modes for enhancing the structural assignment of lipid species. The electrospray ionization source settings for ion mobility were the same as described above. The travelling wave velocity was set to 650 m s^{-1} and the wave height was 40 V. The helium gas flow in the helium cell region of the ion-mobility spectrometry cell was set to 180 ml min^{-1}. Nitrogen, used as the drift gas, was held at a flow rate of 90 ml min^{-1} in the ion-mobility spectrometry cell. The low collision energy was set to 4 eV and the high collision energy was ramped from 25 to 60 eV in the transfer region of the T-Wave device to induce the fragmentation of mobility-separated precursor ions.

Lipidomic data preprocessing and analysis

The structural elucidation and validation of significant features were firstly obtained by searching monoisotopic masses against the available online databases, such as METLIN, Lipid MAPS and HMDB with a mass tolerance of 5 ppm. Fragment ion information obtained by tandem MS (UPLC–HDMSE) was used for the further structural elucidation of significantly changed lipid species. HDMSE data were processed using MSE data viewer (version 1.3, Waters Corp.). Raw data files were processed in Progenesis QI software. Multivariate and univariate statistical analyses were performed using MetaboAnalyst (version 5.0) and also in an R environment. Group differences were calculated using one-way ANOVA. P values were corrected for multiple hypothesis testing and a FDR of 0.05 or less was considered significant.

RNA sequencing and data analysis

Three independent biological replicates per treatment were performed. HEK-293 cells were seeded at a density of $1x10^6$ cells/well in 6 well-plates (Cat# 3335, Corning). After 90 min, cells were treated with vehicle (ethanol) or 50 μM oleic acid. Twenty-four h after seeding, cells were treated with 16 mM FAC for 4 h. Thereafter, the media was removed and cells were washed twice with 0.5 mL PBS. After washing, total RNA was extracted from cells using the AllPrep DNA/RNA Isolation Kit (Cat# 80204, Qiagen). Total RNA was then quantified using a NanoDrop™ Lite Spectrophotometer (Cat# ND-LITE-PR, ThermoFisher).

Upon RNA quality verification, poly-A pull-down was used to enrich mRNAs from total RNA samples, and library construction was performed using Illumina TruSeq chemistry. Libraries were then sequenced using Illumina NovaSeq 6000 at Columbia Genome Center with multiplex samples in each lane, yielding approximately 20M paired-end 100bp reads for each sample. RTA (Illumina) was used for base calling and bcl2fastq2 (version 2.19) for converting BCL to fastq format, coupled with adaptor trimming. Kallisto (version 0.46.1) was used to perform pseudoalignment with bootstrapping to an index created from transcriptomes (Ensembl v96, Human:GRCh38.p13).[72] We tested for differentially expressed genes under various conditions using Sleuth (version 0.30.0), an R package designed to test differential expression between two experimental groups from RNA-seq counts data.[73] Briefly, a likely hood ratio test and a Wald test with b statistic modified to be mathematically equivalent to $\log_2$ of the fold change were performed between two models (null and full) in transcript and gene mode.

Global quantitative proteomics analysis

For global quantitative proteomics of HEK-293 cells, diaPASEF (Data independent acquisition) based proteomics was used.[74] Three independent biological replicates per treatment were performed. In brief, HEK-293 cells were seeded in 100 mm culture dishes at a density of $5x10^6$ per dish (Cat# 430167, Corning). After 90 min, cells were treated with vehicle (ethanol) or 50 μM oleic acid. Twenty-four h after seeding, cells were treated with 16 mM FAC. After 4 h, the media was removed and cells were washed twice with ice-cold PBS (2 mL) to remove the media while keeping the plate on ice. After washing, cells were harvested by trypsinization (1 mL) and transferred to a 5-mL microfuge tube containing 4 mL of culture medium supplemented with 10% SFB. Cells were then pelleted (250 x *g*, 5 min) and resuspended in ice-cold PBS (2 mL). After centrifugation (250 x *g*, 5 min), the cell pellet was stored at -80°C. In the next day. cells were lysed by in lysis buffer (1 % sodium deoxycholate, 100 mM TrisHCl pH 8.5, and protease inhibitors) and boiled for 15 min at 95°C, 1500 rpm.[75] Protein reduction and alkylation of cysteins was performed with 10 mM tris(2-carboxyethyl)phosphine and 40 mM chloroacetamide at 45°C for 10 min followed by sonication in a water bath, cooled down to room temperature. Protein digestion was processed for overnight by adding LysC and trypsin in a 1:50 ratio (μg of enzyme to μg of protein) at 37°C and 1400 rpm. Peptides were acidified by adding 1% trifluoroacetic acid (TFA), vortexed, and subjected to StageTip clean-up via SDB-RPS.[75] Peptides were loaded on one 14-gauge StageTip plugs. Peptides were washed two times with 200 μl 1% TFA 99% ethyl acetate followed 200 μl 0.2% TFA/5%ACN in centrifuge at 3000 rpm, followed by elution with 60 μl of 1% Ammonia, 50% Acetonitrile (ACN) into eppendorf tubes and dried at 45°C in a SpeedVac centrifuge. Samples were resuspended in 10 μl of LC buffer (3% ACN/0.1% FA). Peptide concentrations were determined using NanoDrop and 200 ng of each sample were used for diaPASEF analysis on timsTOFPro. Peptides were separated within 87 min at a flow rate of 400 nl/min on a reversed-phase C18 column with an integrated CaptiveSpray Emitter (25 cm x 75μm, 1.6 μm, IonOpticks). Mobile phases A and B were with 0.1% formic acid in water and 0.1% formic acid in ACN. The fraction of B was linearly increased from 2 to 23% within 60 min, followed by an increase to 35% within 7 min and a further increase to 90% before re-equilibration. The timsTOF Pro was operated in diaPASEF mode[74] and data was acquired at defined 32 × 50 Th isolation windows from m/z 400 to 1,200. The collision energy was ramped linearly as a function of the mobility from 59 eV at 1/K0=1.6 Vs cm^{-2} to 20 eV at 1/K0=0.6 Vs cm^{-2}. The acquired diaPASEF raw files were searched with the UniProt Human proteome database (UP000005640) in the DIA-NN search engine with default settings of the library-free search algorithm.[76] The false discovery rate (FDR) was set to 1% at the peptide precursor and protein level. Statistical analysis of the post DIA-NN labeled normalized abundance

Please cite this article in press as: Mann et al., Ferroptosis inhibition by oleic acid mitigates iron-overload-induced injury, Cell Chemical Biology (2023), https://doi.org/10.1016/j.chembiol.2023.10.012

matrix was performed using the one factor statistical analysis feature of Metaboanalyst (version 5.0). Briefly, the normalized matrix was uploaded, filtered, log transformed, and ANOVA with Fisher's LSD post-hoc performed with correction for multiple hypothesis testing.

C. elegans treatments and mortality rate assessment

Experimental iron overload was induced by treating L4 hermaphrodites with FAC (Cat# F5879, Sigma-Aldrich). In brief, 100-μL aliquots of sterile-filtered FAC dissolved in M9 buffer were spotted onto 32.8 mm Petri dishes (Cat# K13-0035, Kasvi) containing 3 mL NGM and *E. coli* (OP50). NGM agar plates supplemented with FAC (final concentrations ranged from 15 to 145 mM) were made ahead of time 24 h. The next day, approximately 25 hermaphrodites (at the L4 stage) were transferred to vehicle (M9)- or FAC-containing plates. After 48 hours, mortality rate was assessed and alive worms were transferred to fresh compound-treated plates containing 3 mL NGM and OP50. After additional 48 hours (96 h after the beginning of FAC exposure), mortality rate was assessed again. Dead worms were those stopped moving and were unable to respond to harsh touch with a platinum pick, as described previously.[77]

Co-treatments with the anti-ferroptotic agent ferrostatin-1 (Fer-1) (Cat# SML0583, Sigma-Aldrich) or Butylhydroxytoluene (BHT) (Cat# B1215000, Sigma-Aldrich) were performed. Fer-1 or BHT were dissolved in DMSO (Cat# 276855, Sigma-Aldrich) and diluted in M9 prior to plating onto the OP50 food source. Final Fer-1/BHT and DMSO concentrations in plates were 200 μM and 1%, respectively. The Fer-1 solution or vehicle (1% DMSO) was allowed to absorb into the plates for 30 minutes before adding L4 stage nematodes.

In parallel experiments, plates were supplemented with fatty acids (FAs) according to previously described.[49,78] In short, 0.1% Tergitol NP40 (Cat# NP40S, Sigma-Aldrich) was added to liquid NGM media (before solidification). After autoclaving, FAs [stearic acid (18:0; Cat# 00A1030.06.AG, Labsynth), oleic acid (18:1; Cat# 01A1048.01.BJ, Labsynth), linoleic acid (18:2; Cat# W800075, Sigma-Aldrich)] diluted in ethanol were added to liquid NGM media. Plates (32.8 mm Petri dishes, Cat# K13-0035, Kasvi) containing 3 mL NGM agar supplemented with FAs were dried at room temperature for 24 hours and then seeded with OP50. Final FAs and ethanol concentrations in plates were 0.15 mM and 0.1%, respectively. Two days after seeding OP50, L1 synchronized larvae were transferred to the FAs-containing plates. When L4 stage was reached, FAC treatment was performed as described above and mortality rate was assessed after 48 and 96 h.[77]

C11 BODIPY 581/591 (lipid ROS) analysis in *C. elegans*

Worms at L4 stage were treated with 50 mM FAC as described above. In parallel experiments, worms were pretreated with 0.15 mM fatty acids at L1 stage. For details, see "*C. elegans* treatments and mortality rate assessment" (previous item). At 48 h after FAC treatment, worms (~25/group) were collected, washed three times with M9 buffer, and transferred to 0.5 mL tubes (Cat# AB0533, ThermoFisher) containing 0.3 mL of 10 μM C11 BODIPY dissolved in M9 buffer (OP50 was added to stimulate pharyngeal pumping and consequent ingestion of the fluorescent dye). After agitation for 1 h at room temperature, worms were washed three times with M9. To quantify fluorescence, worms were immobilized with 10 mM levamisole and mounted on 2% agarose pad. Confocal microscopy was carried out on a Leica DMI6000 B microscope coupled with TCS SP5 confocal scanner. Images were captured using a 20x/0.70 objective. Oxidized BODIPY581-591-C11 (green fluorescence) were excited at 488 nm and images were collected from emission at 530(30) nm, respectively. Non-oxidized BODIPY581-591-C11 (red fluorescence) were excited at 543 nm and images were collected from emission at 590(30) nm, respectively.[79] Lipid peroxidation index is calculated by the following ratio: [green fluorescence/(green + red) fluorescence]. Data was quantified from 15 worms per group (derived from 3 independent experiments). Images were processed in ImageJ 1.48v (U.S. National Institutes of Health, Bethesda, MD).

Mice treatments and toxicity assessment

Before experimental procedures, the animals underwent a period of 7 days of adaptation to the researchers and the laboratory. Thereafter, animals were randomly (www.random.org) assigned to one of the four experimental groups (7 animals per group): (i) Control; (ii) FAC; (iii) oleic acid; and (iv) FAC + oleic acid. Oleic acid-treated animals were subjected to a 10 days-pretreatment with this fatty acid (Labsynth, Cat# 01A1048.01.BJ; 600 mg/kg/day) by oral route. Oleic acid dose was based on a previous study[80] and its administration was performed based on a previously reported micropipette-guided drug administration method,[81] which allowed for the voluntary ingestion of oleic acid; control animals received only vehicle (60 μL). After 10 days of vehicle or oleic acid treatment, animals received a single intraperitoneal injection of FAC (120 mg/kg, diluted in 0.9% NaCl solution); control animals received only vehicle (0.9% NaCl solution; 10 mL/kg). After 4 h, animals were euthanized by decapitation and whole blood were collected in a 1.5 mL microtube. Following coagulation at 37°C, samples were centrifuged (8 min, 1400 x *g*, 4°C) to obtain serum for further analysis. Alanine aminotransferase (ALT) and lactate dehydrogenase (LDH) in serum were measured by commercial kits (Labtest, Brazil). Liver was collected for measurement of lipid peroxidation through the thiobarbituric acid reactive substances (TBARS) method.[82] One of the 28 animals (from the oleic acid + FAC group) died before completion of the study.

Please cite this article in press as: Mann et al., Ferroptosis inhibition by oleic acid mitigates iron-overload-induced injury, Cell Chemical Biology (2023), https://doi.org/10.1016/j.chembiol.2023.10.012

QUANTIFICATION AND STATISTICAL ANALYSIS

In cell viability analyses, EC_{50} values were using Prism 9.0 (GraphPad Software, La Jolla, CA). Flow cytometry data were processed using FlowJo 10.1r5 (Becton, Dickinson & Company, Ashland, OR). *C. elegans* confocal images were processed in ImageJ 1.48v (U.S. National Institutes of Health, Bethesda, MD).

Graphing and statistical analyses were performed using Prism 9.0. Shapiro-Wilk test was used to determine whether the data had normal (Gaussian) distribution. Unless otherwise stated, data represent the mean ± SD out of at least three independent experiments. The differences were considered significant by one-way or two-way ANOVA followed by Tukey's post-hoc test, $^{*}p < 0.05$, $^{**}p < 0.01$, $^{***}p < 0.001$, $^{****}p < 0.0001$. Details of experiments and additional information concerning statistical tests used can be found in the main text and figure legends.